© 2020. Published by The Company of Biologists Ltd | Development (2020) 147, dev182576. doi:10.1242/dev.182576

STEM CELLS AND REGENERATION

RESEARCH ARTICLE

# Histone variant dictates fate biasing of neural crest cells to melanocyte lineage

**Desingu Ayyappa Raja[1,2], Yogaspoorthi Subramaniam[1,2], Ayush Aggarwal[1,2], Vishvabandhu Gotherwal[1,2], Aswini Babu[1], Jyoti Tanwar[1,2], Rajender K. Motiani[1,‡], Sridhar Sivasubbu[1], Rajesh S. Gokhale[1,*] and Vivek T. Natarajan[1,2,¶]**

## ABSTRACT

In the neural crest lineage, progressive fate restriction and stem cell assignment are crucial for both development and regeneration. Whereas fate commitment events have distinct transcriptional footprints, fate biasing is often transitory and metastable, and is thought to be moulded by epigenetic programmes. Therefore, the molecular basis of specification is difficult to define. In this study, we established a role for a histone variant, *H2a.z.2*, in specification of the melanocyte lineage from multipotent neural crest cells. *H2a.z.2* silencing reduces the number of melanocyte precursors in developing zebrafish embryos and from mouse embryonic stem cells *in vitro*. We demonstrate that this histone variant occupies nucleosomes in the promoter of the key melanocyte determinant *mitf*, and enhances its induction. CRISPR/Cas9-based targeted mutagenesis of this gene in zebrafish drastically reduces adult melanocytes, as well as their regeneration. Thereby, our study establishes the role of a histone variant upstream of the core gene regulatory network in the neural crest lineage. This epigenetic mark is a key determinant of cell fate and facilitates gene activation by external instructive signals, thereby establishing melanocyte fate identity.

**KEY WORDS: Histone variant, Melanocyte, Gene regulatory network, Epigenetic regulation, Fate-bias, Specification, Pigmentation**

## INTRODUCTION

Cell fate determination is driven by a cascade of transcription factors (TFs) that are governed by external cues (Kawakami and Fisher, 2011; Martik and Bronner, 2017). The neural crest sets a paradigm for stem cell multipotency and lineage specification, and serves as a model for understanding fate decisions. Recent data emerging from single-cell transcriptomics of neural crest cells (NCCs) demonstrates the emergence of fate bias or specification that further unfolds to culminate in fate commitment (Soldatov et al., 2019) or determination. NCCs and NCC-derived progenitor populations give rise to melanocytes during embryonic development and adult skin homeostasis and regeneration, respectively (White and Zon, 2008). The ability to trace cells visually, combined with the extensive literature on gene regulatory networks, render melanocytes as the preferred choice to trace the mechanisms behind fate decisions.

Almost all aspects of melanocyte biology, from lineage commitment to differentiation, are controlled by the central TF MITF (Goding and Meyskens, 2006; Kawakami and Fisher, 2017). WNT and BMP signalling (Jin et al., 2001; Takeda et al., 2000), and downstream TFs SOX10 (Marathe et al., 2017), PAX3 (Watanabe et al., 1998), FOXD3 (Kos et al., 2001) and LEF1 (Dunn et al., 2000), form the core of gene regulatory networks that control *mitf* induction and mediate melanocyte specification and determination. Although the upstream instructive signals and downstream orchestrators are well appreciated, cell-intrinsic modulators that mediate specification events remain obscure. Epigenetic mechanisms that alter chromatin accessibility could provide an intervening regulatory layer and are likely to play a key role in determining the fate of NCC lineages.

Epigenetic regulators, including the histone deacetylase HDAC1 (Ignatius et al., 2008, 2013), which is involved in locus-specific histone deacetylation; the DNA methyl transferase DNMT3b, which causes base methylation (Rai et al., 2010); and the histone variant H3.3, which replaces the core histone H3, are all involved in the derivation of specific cell types from NCCs (Cox et al., 2012). Another histone variant, H2A.Z, encoded by two genes, *H2a.z.1* and *H2a.z.2*, has been implicated in NCC differentiation (Pünzeler et al., 2017; Sivasubbu et al., 2006). Recent studies demonstrate the crucial role of H2A.Z in human metastatic melanoma survival and proliferation (Vardabasso et al., 2015), and the involvement of the H2A.Z chaperone PWWP2A in NCC differentiation (Pünzeler et al., 2017). Another recent study demonstrates a selective role for *H2A.Z.2* in craniofacial morphogenesis with implications for the congenital disorder Floating Harbor Syndrome (Greenberg et al., 2019). In addition, melanomas recapitulate neural crest fate (Kaufman et al., 2016). Therefore, it is possible that histone variants dictate the fate of melanocytes from neural crest-derived progenitors.

In this study, using zebrafish as well as mouse embryonic stem cell-derived melanocyte models, we demonstrate a selective role for H2A.Z.2 in the fate-biasing of NCCs to melanocytes. Furthermore, we show that this variant occupies the promoter of *mitf* and its upstream regulator *sox9*, and governs the inducibility of *mitf* under appropriate cues. CRISPR-targeted mutation in *h2a.z.2* reinforces its central role during pigmentation and the related process of melanocyte regeneration in adult zebrafish. Thereby, we establish the selective role of a histone variant upstream of the TF network that enables cell-intrinsic responsiveness to external instructive signals. Our study adds a new dimension to the recent developments in tracing the lineage map of NCC derivatives and provides a molecular basis for the fate bias observed during specification.

[1]Pigment Cell Biology Group, CSIR-Institute of Genomics and Integrative Biology, Mathura Road, New Delhi, 110025, India. [2]Academy of Scientific and Innovative Research, Kamla Nehru Nagar, Ghaziabad, Uttar Pradesh, 201002, India.
*Present address: National Institute of Immunology, Aruna Asaf Ali Marg, New Delhi, India. ‡Present address: Laboratory of Calciomics and Systemic Pathophysiology, Regional Centre for Biotechnology, Faridabad, Haryana 121001, India.

¶Author for correspondence (tnvivek@igib.in; tn.vivek@igib.res.in)

V.T.N., 0000-0002-8537-5471

**Received 15 July 2019; Accepted 24 January 2020**

Development (2020) 147, dev182576. doi:10.1242/dev.182576

## RESULTS

### The histone variant, H2A.Z.2 but not H2A.Z.1, is involved in the derivation of melanocytes in zebrafish

Across vertebrates, the histone variant H2A.Z is encoded by two distinct paralogs, H2A.Z.1 (Z1) and H2A.Z.2 (Z2), that are around 97% identical at the protein level and are therefore difficult to distinguish experimentally (Dryhurst et al., 2009; Matsuda et al., 2010). In zebrafish, these two genes are named as *h2az2b* and *h2az2a*, respectively. In this study, for the sake of uniformity and simplicity, these are referred to as h2az.1 or Z1, and h2az.2 or Z2 across mice as well as zebrafish. The disruption of Z1 is not compensated for by intact Z2 and the knockout mouse embryos fail to survive (Faast et al., 2001). Therefore, to decipher their individual contribution to the differentiation of NCCs, especially to melanocytes, we adopted a morpholino (MO)-based transient knockdown strategy in developing zebrafish embryos. Knockdown of Z1 resulted in gross embryonic deformities and poor development being observed, as has also been reported previously (Greenberg et al., 2019; Madakashira et al., 2017; Murphy et al., 2018; Sivasubbu et al., 2006). Z2 morphants exhibited milder effects with regards to their gross morphology but they presented a drastic reduction in pigmentation (Fig. 1A-D).

The pigmentation phenotype of Z2 MO could be recapitulated using a splice block MO targeted to Z2, and also upon co-injection of Z2 MO with p53 MO, reiterating the specific nature of the phenotype (Fig. S1). Furthermore, analysis of recent single-cell sequencing studies (Saunders et al., 2019) confirmed the expression of Z1 and Z2 in lineages arising out of the neural crest that result in melanocytes (Fig. S2). Upon co-injection of Z2 MO along with mouse *H2a.z.1* or *H2a.z.2* mRNAs, a rescue of around 50% was observed only for *H2a.z.2* mRNA (Fig. 1E). Thereby, it was demonstrated that Z2 has a distinct pigmentation role and is not compensated for by an increased dosage of Z1. To decipher the determinants that contribute to the Z2 selectivity, we performed single amino acid changes by site-directed mutagenesis of the three involved residues. Whereas $H2AZ.2_{A14T}$ and $H2AZ.2_{A127V}$ were able to rescue head melanophore numbers to a level comparable with the wild-type H2AZ.2, $H2AZ.2_{T38S}$ was only capable of a partial rescue (Fig. S3).

### *h2a.z.2* depletion selectively reduces melanocyte numbers

The characteristic reduction in pigmentation of Z2 morphants could be either due to decreased pigment production or due to the absence of mature pigmented cells. At 2 days postfertilization (dpf), we observed a severe reduction in the number of ftyrp1:$GFP^+$ cells in Z2 morphants, notably in the dorsal as well as the ventral pool of melanocytes above the yolk sac, clearly indicating that the number of melanocytes is affected (Fig. 1B). Additionally, at 7 dpf, the lateral line melanocytes were reduced in Z2 morphants, suggesting that the progenitor pool may be affected (Fig. 1C). We therefore used various transgenic reporter lines from the neural crest to the melanocyte lineage to estimate respective cell numbers at different stages of development (Fig. 1F). We observed that Z2 morphants displayed a 45-50% reduction in differentiating/differentiated melanophores and a 30% reduction in melanoblast numbers (Fig. 1F). However, the $sox10^+$ progenitor population remained unaffected in Z2 morphants. Therefore, h2a.z.2 is likely to play a key role in the lineage commitment of melanocytes from neural crest-derived progenitors.

### h2a.z.2 dictates melanocyte and glial footprint in NCCs

Multipotent NCCs progressively undergo the process of fate specification and determination to give rise to melanocytes, craniofacial cartilage, adipocytes, smooth muscle cells, Schwann cells and neurons (Donoghue et al., 2008; Le Douarin et al., 2004). Based on whole mount *in situ* hybridization (WISH), we observed that the early neural crest gene expression of *foxd3*, *sox10*, *crestin* and *tfap2a* were not decreased in Z2 morphants (Fig. 1G,H). This indicates that depletion of *h2a.z.2* could selectively affect a subpopulation of NCC-derived progenitors from which melanocytes, and possibly a few other cell types, would be derived. Hence, we resorted to identifying gene expression changes in this seemingly homogeneous population that could explain decreased melanocyte numbers.

We created Z2 morphants in a *Tg(sox10:GFP)* line and sorted the $GFP^+$ cells at 16-18 hpf. At this time point, neural crest-derived sox10 expression is retained and also lineage-specific differentiation markers begin to emerge and the cell fate identity is established (Curran et al., 2010; Wagner et al., 2018). Microarray and pathway enrichment analysis of the $GFP^+$ cells revealed that the set of downregulated genes mapped to developmental pigmentation-related processes (Fig. 2A-C). Targeted analysis of the data indicated reduced expression of TFs with a known role in the melanocyte lineage, such as *mitfa*, *tfap2a*, *tfap2e* and *sox9b*, as well as melanocyte migration and survival factors, such as *kita* and *ednrb1a*. Similarly, we also observed decreased expression of glial lineage TFs such as *nfatc4*, *pax7* and *lmo4*. However, the neuronal lineage TFs, such as *foxo1*, *foxo3* and *sox8*, were upregulated in the Z2 morphants (Fig. 2D). As these are gene expression changes in the isolated $sox10^+$ cells, we interpret the decreased expression to indicate alterations in the subpopulations of differentiating cells derived from the NCCs.

To verify the reduction in specific cell types, we adopted WISH for lineage-specific differentiation markers and analysis of cell type-specific transgenic lines that label NCC derivatives. *dct* and *c-kit*, which label melanocytes, showed decreased staining in the Z2 morphants (Fig. 2E). A similar pattern of decreased staining was observed for differentiated Schwann cells using the markers *krox20* and *mbp*, which labelled the lateral line-associated glial cells (Fig. 2F). The number of undifferentiated Schwann cells, visualized by *Tg(foxD3:GFP)*, was substantially reduced (Fig. 2F). *Tg(nbt:DsRed)*-marked enteric neurons remained unaffected (Fig. S4) and similarly WISH for *isl2a* showed no change (Fig. 2G). However, we observed the presence of ectopic neurons in the trunk, above the spinal cord neuron bundle, which suggested a local increase in the neuronal population (Fig. 2G and Fig. S4). Labelling by *Tg(sox10:GFP)*, as well as Alcian Blue staining of craniofacial appendages and fin cartilage, showed no major changes, suggesting normal cartilage specification. However, we noticed a consistent decrease in jaw area as a result of defective ceratobranchial appendage spacing and a mild increase in the angle of the ceratobranchial cartilage (Fig. S4). Altogether, our data suggest that h2a.z.2 plays a selective role in the derivation of melanocytes and glial populations from the NCC. Interestingly, previous studies have shown that these two cell types emerge from a common progenitor (Raible and Eisen, 1994).

### h2a.z.2 functions in conjunction with mitfa to control melanocyte derivation

Based on temperature-sensitive mutants, Micropthalmia-associated TF *mitfa*, is seemingly dispensable for specification (Johnson et al., 2011). However, mitfa is the earliest known marker of lineage commitment that controls the expression of downstream identity genes involved in melanocyte fate determination (Goding, 2000; Lister et al., 1999). Indeed, we observed a decrease in *mitfa* expression in $sox10^+$ cells, and this was further corroborated by the

Development (2020) 147, dev182576. doi:10.1242/dev.182576

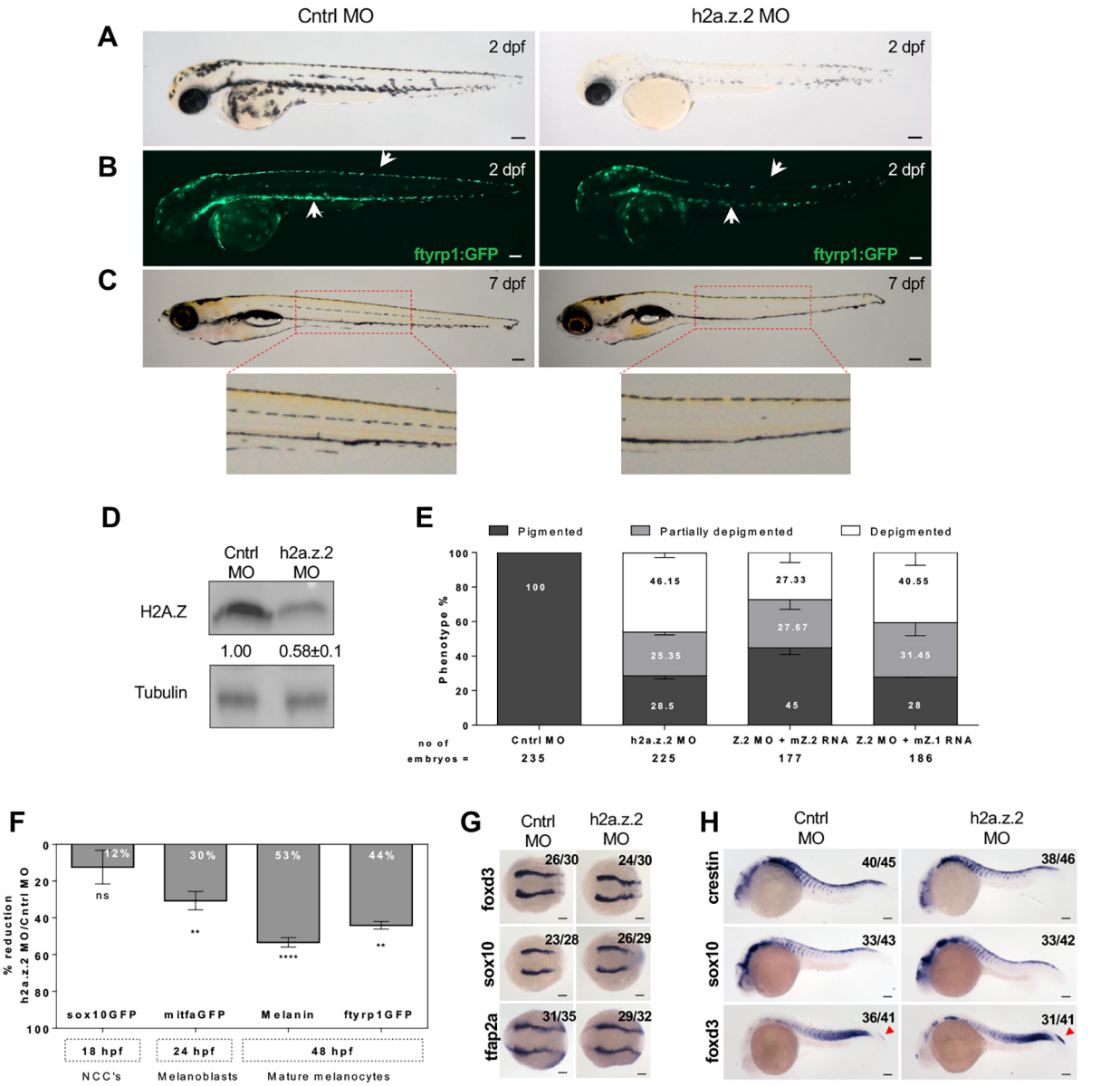


**Fig. 1. *H2a.z.2* controls melanocyte numbers during zebrafish development.** (A) Bright-field images of control MO- and H2a.z.2 MO-injected embryos (Z2 MO) at 2 days postfertilization (dpf). (B) Fluorescence images of *Tg(ftyrp1:GFP)* that tags differentiating melanophores, in control and Z2 MO embryos at 2 dpf. White arrows indicate the dorsal and ventral stripe of melanophores. (C) Bright-field images of control and Z2 MO at 7 dpf. Insets show enlarged views of the lateral line melanophores. (D) Western blot analysis of control and Z2 MO embryos at 2 dpf, carried out using an antibody that recognizes both H2A.Z.1 and H2A.Z.2 proteins, referred to together as H2AZ. Numbers refer to fold change normalized to H3. (E) Bar graphs represent mean±s.e.m. percentage of embryos with varying degrees of pigmentation: depigmented (<20 head melanophores), partially pigmented (21-39 head melanophores) and normally pigmented (40 and above). These were scored manually at 2 dpf, from embryos injected with control MO, Z2 MO, Z2 MO along with mouse *H2a.z.1* mRNA or mouse *H2a.z.2* mRNA across three independent biological replicates. Number of embryos analysed is given under the bars. (F) Inverted bar graphs represent mean±s.e.m. ($n$=3) percentage reduction in cell numbers of Z2 MO, compared with the control, in various marker lines. Time of assessment of labelled cells, their identity and the transgenic line used are indicated. (G) Whole-mount RNA *in situ* hybridization (WISH) assay showing the expression pattern of early neural crest markers *foxd3*, *sox10* and *tfap2a* at 11 hpf. The assay resulted in the staining of migrating neural crest cells, which remained unaltered in the Z2 MO. (H) WISH-based expression pattern of neural crest markers *crestin*, *sox10* and *foxd3* at 24 hpf. Arrowheads in the *foxd3* panel indicate tail tip neural crest cells. The numbers in the WISH images indicate frequency of the represented phenotype in the total number of embryos analysed. Scale bars: 100 µm.

transgenic line mitfa:GFP and WISH staining for *mitfa* (Fig. 3A). Messenger RNA levels of *mitfa* were observed to be around 50% in the Z2 MO (Fig. 3B). Therefore, we set out to decipher the interplay of h2a.z.2 and mitfa in mediating melanocyte lineage commitment. A marked rescue in the melanocyte counts of *mitfa* mRNA-injected Z2 morphants was noted (Fig. 3C,D). To confirm the gene-selective elevation of mitfa by the two H2A.Z variants, we expressed the mouse orthologues by way of RNA injections. Western blot analysis indicated that the two variants exhibited comparable levels of expression but only Z2 enhanced the *mitfa* expression detected by WISH staining at 24 hpf (Fig. 3E,F). These observations confirmed the genetic interaction between h2a.z.2 and mitfa. Furthermore, h2a.z.2 likely functions upstream of mitfa and hence could modulate melanocyte fate.

Development (2020) 147, dev182576. doi:10.1242/dev.182576

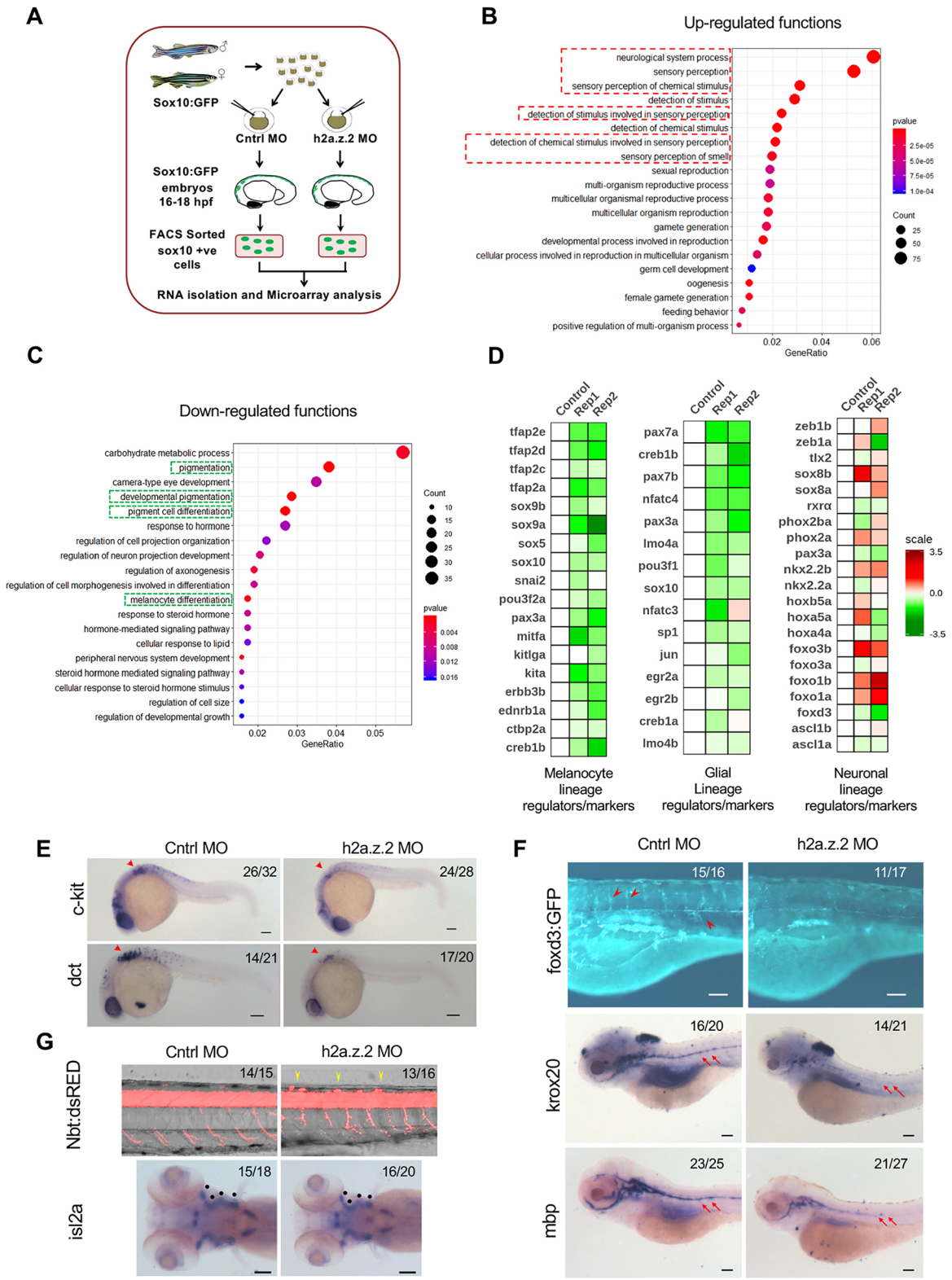


**Fig. 2. *H2a.z.2* alters the neural crest gene regulatory network and decreases the melanocyte and glial footprint.** (A) Schematic design of the microarray experiment. (B,C) Bubble plots representing gene ontology functions of differentially regulated genes with a $\log_2$ fold change $\leq -0.6$ (downregulated, B) and $\geq 0.6$ (upregulated, C) upon the silencing of Z2 in *sox10*$^+$ cells. (D) Heatmaps representing differential expression of key transcription factors and lineage markers in *sox10*$^+$ cells of Z2 MO compared with the control across melanocyte, glial and neuronal lineages. (E) WISH-based expression pattern of melanocyte markers c-*kit* and *dct* at 24 hpf. Arrowhead represents vagal melanocytes. (F) Top: *Tg*( *foxd3*:GFP) labelling of glial cells that mark undifferentiated glia. Red arrowheads show cell population of interest. Middle and bottom: WISH of glial markers *krox20* and *mbp* at 5 dpf. Red arrows indicate the glial lateral line. (G) Top: *Tg*(*nbt*:dsRed) labelling of neurons in the spinal cord bundle (lateral view). Yellow arrowheads mark the ectopic neurons. Bottom: WISH of the cranial motor neuron *isl2a*. Black dots represent motor neurons that arise from neural crest cells. The numbers in the top right corners of E, F and G indicate number of embryos with observed phenotypes/total number of embryos analysed. Scale bars: 100 µm.

Development (2020) 147, dev182576. doi:10.1242/dev.182576

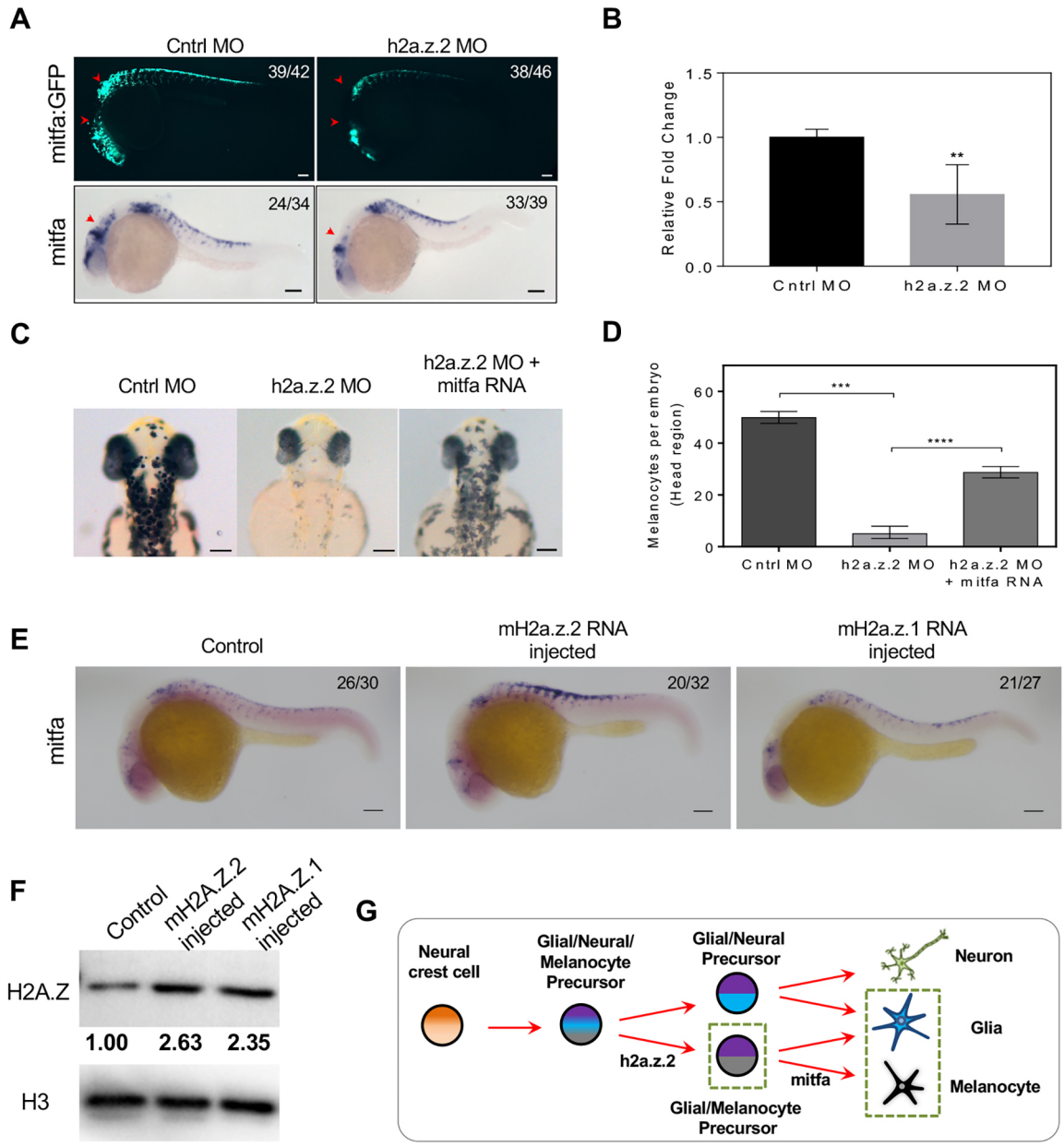


**Fig. 3. *H2a.z.2* genetically interacts with *mitf* during melanocyte specification.** (A) Top: Tg(*mitfa*:GFP) labelling of melanocytes. Red arrowheads indicate cranial and vagal melanocytes. Bottom: WISH of *mitfa* at 24 hpf. Red arrowheads indicate cranial melanocytes. (B) Real-time quantification of *mitfa* RNA upon Z2 MO indicates a ~0.5-$\log_2$ fold downregulation in expression. Bars represent mean±s.e.m. across three independent biological replicates with ~50 embryos each. (C) Bright-field images of control, Z2 MO and Z2 MO, co-injected with *mitfa* mRNA at 48 hpf, showing head melanophores. (D) Quantification of the rescue of head melanophore numbers upon *mitfa* RNA co-injection. Bars represent geometric mean with 95% CI of the number of head melanophores with at least 30 embryos each. (E) *mitfa* WISH at 24 hpf upon RNA injection of mouse H2a.z.2 or H2a.z.1, compared with the noninjected control. (F) Western blot analysis of H2AZ protein in noninjected or mouse H2a.z.2 or H2a.z.1 RNA-injected embryos, normalized to total H3 protein. (G) Schematic representation of the neural crest-derived lineages, highlighting the dependence of melanocyte and glial cells on *h2a.z.2*. The numbers in the WISH images indicate frequency of the represented phenotype in the total number of embryos analysed. Scale bars: 100 µm.

### The derivation of melanocytes from mouse embryonic stem cells is controlled by *H2a.z.2*

Our experiments suggested that it is likely that h2a.z.2 plays a role in the specification/determination of an upstream progenitor population from which melanocytes arise. Additionally, the decrease in glia in the h2a.z.2 morphant indicated that the bipotent progenitor of melanocytes and glial populations could be affected. Furthermore, an increase in neurons is suggestive of a compensatory increase in neuronal progenitors. Our observations therefore indicate a hierarchical model of fate determination in the NCCs, which is in tune with recent studies (Le Douarin and Dupin, 2003; Raible and Eisen, 1994; Soldatov et al., 2019). We propose a model, wherein h2a.z.2 operates at the level of the tripotent glial/neuronal/melanocyte progenitor in specifying a melanocyte/glial fate (Fig. 3G).

Although the zebrafish-based experiments helped us to narrow down the function of this variant in melanocyte derivation, cellular and molecular insights are required to establish its role in specification. To understand this molecular mechanistic link, we established a method to derive melanocytes from R1/E mouse embryonic stem cells (mESCs), wherein the mESCs were converted to melanocytes through an intermediate embryoid body (EB) state (Fig. 4A). Herein, we observed ~45% of the cells to be $SOX10^+$ and

Development (2020) 147, dev182576. doi:10.1242/dev.182576

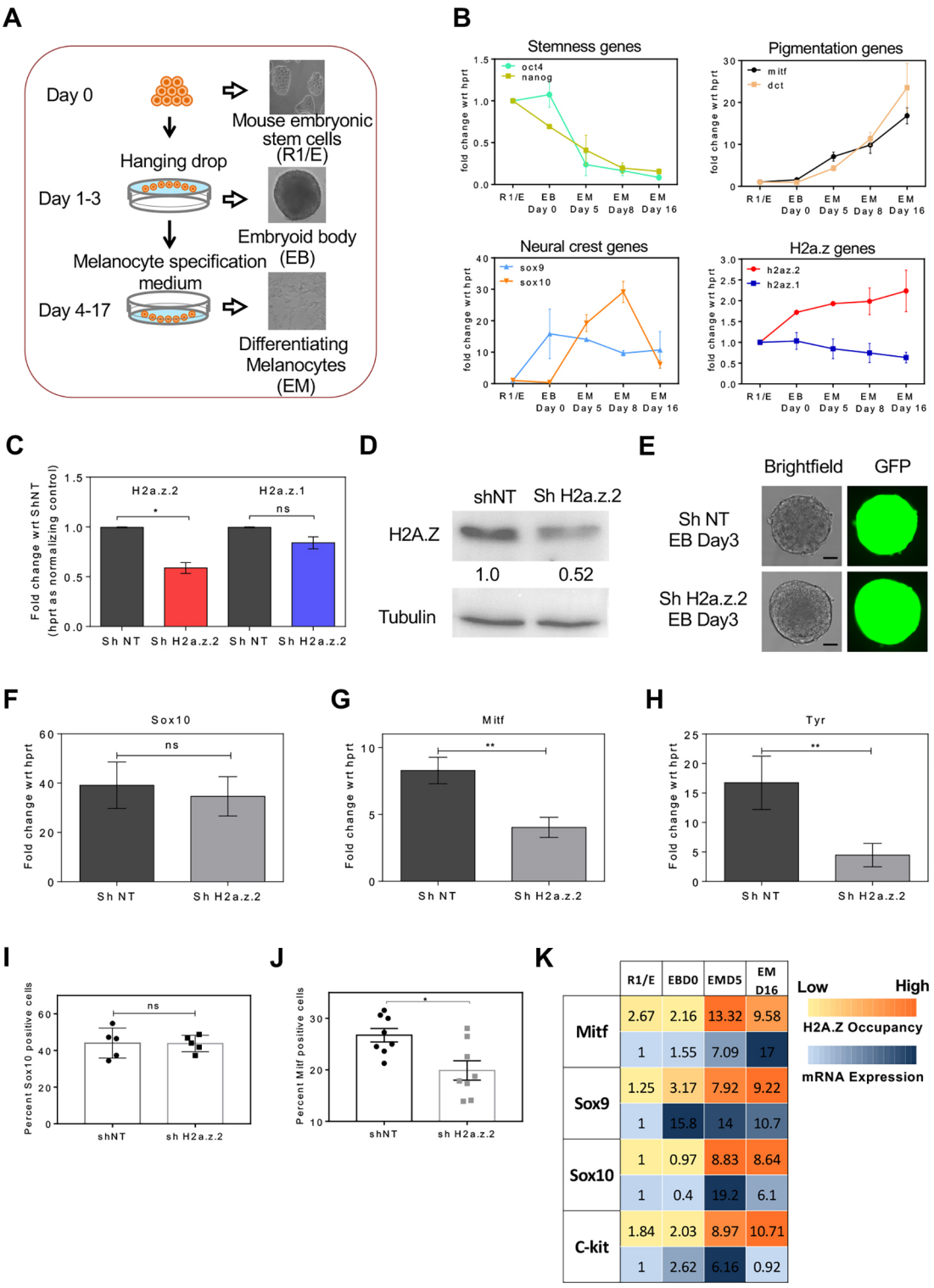


**Fig. 4. *H2.a.z.2* controls melanocyte derivation from mouse embryonic stem cells *in vitro*.** (A) Schematic of melanocyte derivation from mouse R1/E stem cells. (B) Kinetics of expression patterns of stemness genes (*oct4* and *nanog*); pigmentation genes (mitfand *dct*); neural crest genes (*sox9* and *sox10*); and *H2a.z.1* and *H2a.z.2*, at different stages of melanocyte derivation from mouse R1/E stem cells. (C) Bar graphs representing qRT-PCR for *H2.a.z.1* (blue) and *H2.a.z.2* (Ignatius et al., 2013) in shZ2 cells compared with shNT at the embryoid body (EB) stage. (D) Western blot analysis of H2AZ in control- (ShNT) and H2A.Z-silenced (ShZ2) cells. The numbers represent fold change normalized to tubulin with respect to the control. (E) Bright field and GFP images of EBs derived from R1/E cells silenced using a lentiviral construct for nontargeting or Z2 shRNA, encoding a GFP marker. (F-H) Bar graphs representing qRT-PCR analysis for *sox10*, *mitf* and *tyr* (tyrosinase) 6 days postinduction of differentiation. Bars represent mean±s.e.m. (*n*=3) of the fold change. (I) Bar graph representing the percentage of cells positive for Sox10 on day 10 of differentiation. *n*=500 cells. (J) Bar graph representing the percentage of cells positive for Mitf on day 10 of differentiation (*n*=500 cells). (K) Heatmap representing the promoter occupancy of H2AZ (*H2A.Z.1* and *H2A.Z.2*) determined by Chromatin Immunoprecipitation (ChIP) and the corresponding mRNA levels of *mitf*, *sox9*, *sox10* and *c-kit* during various stages of melanocyte derivation from R1/E cells. The numbers in the heatmap represent the percentage of enrichment of H2A.Z occupancy in ChIP and fold change compared with the mRNA levels of R1/E cells as determined by qRT-PCR.

Development (2020) 147, dev182576. doi:10.1242/dev.182576

around 25% to be MITF$^+$, confirming the derivation of melanocytes in this model (Fig. S5). Targeted gene expression analysis of NCC, melanocyte and stemness-related genes were performed at different days of melanocyte formation (Fig. 4B). As anticipated, the expression of *Mitf* was induced at day 5 and further increased until day 16. Similarly, we observed that the expression of the pigmentation gene *Dct* was induced during the course of the experiment. We noticed that the expression of stemness factors *Oct4* and *Nanog* were drastically reduced during the course of induction, suggesting that the cells are undergoing differentiation. Strikingly, the expression patterns of *H2a.z.2* and *H2a.z.1* were opposite to each other. Whereas the expression of *H2a.z.2* was positively correlated with melanocyte specification, the expression of *H2a.z.1* was decreased. This pattern of *H2a.z.1* expression was similar to that of the stemness factors *Oct4* and *Nanog*.

To illustrate the functional role of H2a.z.2 in mESCs, we silenced H2a.z.2 and studied melanocyte derivation. In the cells stably expressing short hairpin RNA that targets H2a.z.2 (shZ2), a reduction of ∼50% in *H2a.z.2* mRNA levels could be observed, whereas *H2a.z.1* levels remained unaltered (Fig. 4C). The total reduction in H2AZ protein was ∼50% upon Z2 silencing (Fig. 4D). Interestingly, previous studies report that knockdown of *H2a.z.1* in embryonic stem cells leads to the formation of defective EBs with irregular structural integrity (Hu et al., 2013). We did not observe significant difference in the size and morphology of the *H2a.z.2*-depleted EBs (Fig. 4E), further strengthening the case for a differential role for the two proteins, at least during early developmental stages.

Upon the induction of melanocytes from R1/E cells stably expressing shZ2, the expression of the neural crest gene *Sox10* remained unaltered when compared with nontargeting shRNA (shNT) (Fig. 4F). This observation is strikingly similar to the Z2 MO scenario in zebrafish embryos where a significant decrease in the mRNA levels of the master TF *mitf* and its target gene *Tyr*, in shZ2 cells, was noted when compared with shNT cells (Fig. 4G,H). Although the number of Sox10$^+$ cells did not differ, we observed a 30% decrease in the Mitf$^+$ cells upon Z2 silencing (Fig. 4I,J), thus, highlighting a conserved role for H2a.z.2 in melanocyte specification across zebrafish and mouse. Having established the cell-based model of melanocyte specification and the effect of H2a.z.2 in the derivation of melanocytes in this model, we set out to identify effectors and the mechanism by which H2a.z.2 could mediate melanocyte specification.

### H2A.Z.2 occupies *Sox9* and *Mitf* promoters, and controls *Mitf* inducibility

Both H2A.Z.1 and H2A.Z.2 occupy the nucleosomes in the promoter as well as enhancer regions immediate to the transcription start site (TSS) of the downstream genes. This occupancy can either facilitate (Bargaje et al., 2012; Gevry et al., 2009; Zovkic et al., 2014) or repress (Dai et al., 2017; Hardy et al., 2009) transcription in a context- and a model system-dependent manner. Partly, this discrepancy could be attributed to the near-identical proteins that are indistinguishable in chromatin immunoprecipitation (ChIP) studies and to the complex nature of chromatin changes brought about by H2A.Z. We therefore employed a silencing strategy followed by ChIP to address the molecular mechanism selective to Z2.

H2A.Z ChIP followed by qPCR for the promoter proximal nucleosomes of Mitf, and other crucial upstream effectors Sox9, Sox10 and Ckit, was performed across various stages of melanocyte specification in the mESC model. We then compared the nucleosome occupancy of H2A.Z to their mRNA level changes at these stages of differentiation. All of these four promoters showed increased occupancy during the course of melanocyte formation from mESCs. Interestingly, we observed that mRNA expression of *Mitf*, positively correlated with the occupancy of H2A.Z (H2A.Z.1+H2A.Z.2) in its promoter, suggesting that H2A.Z facilitates the induction of *Mitf* expression, possibly by modulating the accessibility of the Mitf promoter (Fig. 4K).

Although our progressive induction model provided a window to assess kinetic changes in promoter occupancy, heterogeneity in the cell populations arising during the course of melanocyte induction, limited our interpretations. Therefore, we employed a complementary approach wherein we utilized murine B16 melanoma cells that would represent specified melanocytes. ChIP with an H2A.Z antibody was carried out in B16 cells to check the occupancy in promoter regions of genes related to Mitf, and upstream regulators as well as genes downstream of it in melanocytes. Mitf and Sox9 promoters showed considerable enrichment of 5-7% over input (Fig. 5A), suggesting that these genes might be under H2A.Z control. In contrast, several pigmentation genes such as *Dct*, *Tyr*, *Tyrp1* and *Sox10*, were not enriched for H2A.Z in B16 cells. This is in tune with previous studies on H2A.Z in human melanoma cells (Vardabasso et al., 2015) and our meta-analysis further corroborated this observation (Fig. S6).

Knockdown of H2a.z.2 in B16 cells with siRNA resulted in a consistent 70-80% decrease in mRNA levels of *H2a.z.2*, whereas *H2a.z.1* levels remained unchanged (Fig. S7). H2A.Z ChIP-qPCR was carried out for Sox10, Sox9 and Mitf promoter regions in H2a.z.2 knockdown B16 cells (Fig. 5B,D,F). We observed decreased occupancy of H2A.Z upon Z2 knockdown. A correlated decrease in mRNA expression of *Mitf* and *Sox9* (Fig. 5E,G) suggested that this was a direct consequence of decreased Z2 occupancy. In contrast, the Sox10 promoter, which had minimal occupancy in B16 cells, showed no change upon H2a.z.2 silencing. Correspondingly, the *Sox10* mRNA levels remained unaltered (Fig. 5C). To probe the role of Z2 in the dynamic regulation of Mitf expression, we performed H2AZ ChIP of the Mitf promoter. Upon α-MSH stimulation, which increased mitf RNA levels approximately twofold, an increase in H2AZ occupancy of ∼3.5-fold was observed (Fig. 5H,I). Furthermore, Mitf promoter activity was downregulated upon silencing H2A.Z.2 under basal and α-MSH inducible conditions (Fig. 5J). The effect of H2A.Z2 occupancy on the Mitf promoter was addressed in a reporter assay with the overexpression of H2a.z.2 in B16 cells. Although there was no change in the Mitf promoter activity under basal conditions in Z2-overexpressing cells, α-MSH stimulation resulted in a sevenfold upregulation, which was much higher than the empty vector control transfected cells (Fig. 5K,L). A probable confounder could be the inefficient chromatinization of the reporter construct. To address this, we generated a stable line in B16 cells. Overexpression of Z1 and Z2 followed by stimulation with α-MSH confirmed a Z2-selective inducibility (Fig. S7). Taking these results into account, we conclude that Z2 modulates the promoter region of MITF and facilitates its induction, the absence of which leads to decreased Mitf expression resulting in a reduced number of specified melanocytes.

Occupancy of H2A.Z.2 renders the chromatin state of the promoter to be responsive to upstream activating signals. The role of H2A.Z.2 delineated in the current study, shows a striking similarity with its role in the brain, whereby the incorporation of H2A.Z mediates dynamic gene expression changes associated with memory formation (Zovkic et al., 2014). It is also interesting to

Development (2020) 147, dev182576. doi:10.1242/dev.182576

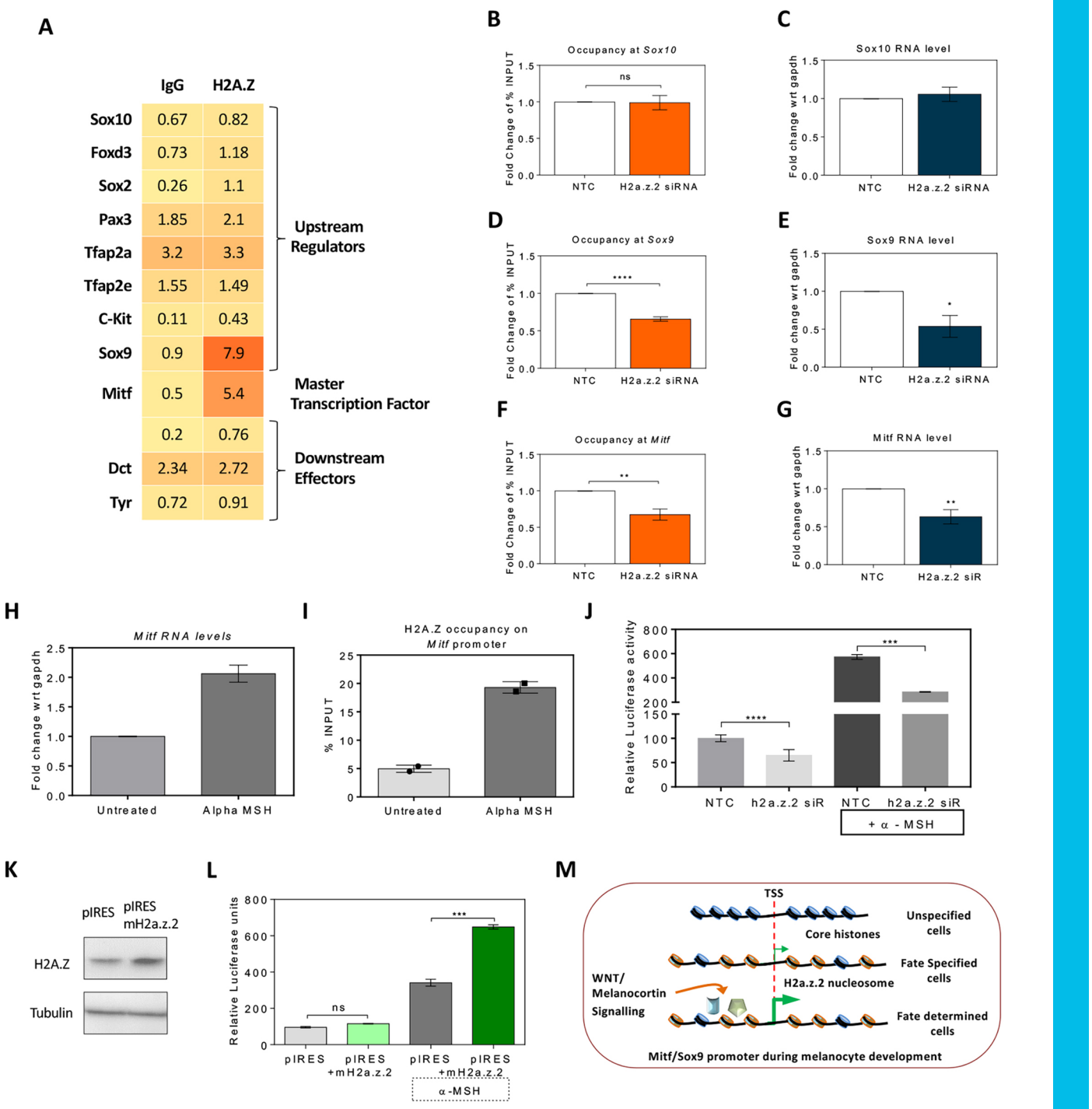


**Fig. 5. H2A.Z.2 occupancy at the Mitf promoter dynamically alters promoter activity.** (A) H2A.Z occupancy at the indicated promoters in melanocytes (depigmented B16 cells) is represented as a heatmap of the percentage input for H2.A.Z as well as normal rabbit IgG. Numbers in the heatmap represent the percentage of enrichment of the promoter DNA in H2A.Z or IgG ChIP. (B,D,F) H2A.Z ChIP of *sox10*, *sox9* and *mitf* promoters upon Z2 knockdown. Bars represent mean±s.e.m. ($n$=3). (C,E,G) mRNA levels of *sox10*, *sox9* and *mitf* upon Z2 knockdown. Bars represent mean±s.e.m. ($n$=3). (H) Bar graph represents mean±s.e.m. of *mitf* RNA levels upon α-MSH stimulation ($n$=5). (I) H2AZ occupancy on the Mitf promoter upon α-MSH stimulation. Bars represent mean±s.d. across independent replicates. (J) Reporter assays for the *mitf* promoter by dual luciferase assay in control- and H2.a.z.2-silenced cells in basal as well as α-melanocyte stimulating hormone (α-MSH)-treated B16 cells for 24 h. Bar graphs represent mean±s.e.m. ($n$=3). (K) Western blot analysis for H2A.Z upon Z2 overexpression. (L) Reporter assays for the *mitf* promoter by dual luciferase assay in control and H2.a.z.2-overexpressing cells in basal as well as α-MSH-treated B16 cells for 24 h. Bar graphs represent mean±s.e.m. ($n$=3). (M) Schematic of the role of *H2.a.z.2* in modulating the *mitf* promoter.

note that upon Z2 silencing in the zebrafish system, *sox9a* and *sox9b* are reduced in the NCC populations (Fig. 2D). Given the upstream role of *sox9* as a positive regulator of *mitf* (Passeron et al., 2007), it is likely it may play an additional role in melanocyte specification via *mitf*. Therefore, we have identified a role of the histone variant H2A.Z.2 in the specification of melanocytes from the multipotent NCCs via the activation of a key transcriptional programme downstream of Mitf (Fig. 5M).

Development (2020) 147, dev182576. doi:10.1242/dev.182576

### *H2a.z.2* is required for adult melanocyte regeneration

Targeted knockout of *H2a.z.1* has been attempted in several organisms and found to be embryonically lethal. However, the Z2 variant has not been systematically studied. CRISPR/Cas9-based targeted deletion of *h2a.z.2* in zebrafish resulted in severe lethality and gross deformities (Fig. S8). Genotyping of the *h2a.z.2* locus from these embryos revealed several indels resulting in large-scale disruptions of this gene. Although *h2a.z.2* seems to be essential for early development, we isolated *h2a.z.2* mutant lines by targeting the coding region downstream of the core histone domain, which maps to the C-terminal extension region beyond the αC domain (Fig. 6A). This region is unstructured and is involved in dynamic docking with histone H3/H4 during nucleosome formation (Bönisch et al., 2012). Interestingly, in the mutant line (H2a.z.2$^{Gln125fsX144}$) we observed fewer melanocytes at the embryonic stage 48 hpf (Fig. 6B). Decreased pigmentation could be traced to the juvenile stages as well (Fig. 6C), confirming the partial loss of function and dominant nature of the mutation. Therefore, the CRISPR-based targeted mutagenesis of H2A.Z.2 confirmed the role of this essential protein in specifying melanocyte numbers.

In the adult zebrafish, stripes appeared paler and on closer examination a reduction in melanophore numbers was observed (Fig. 6D). In the adult animal, the role of H2A.Z.2 in specification could be further verified by studying melanocyte regeneration, a process wherein differentiated melanocytes arise from a prespecified progenitor pool and can be experimentally studied using fin-clip experiments (Hultman et al., 2009). The adult zebrafish fin was therefore cut and allowed to regenerate for a week, during which time the quiescent progenitors were stimulated, and underwent the process of differentiation to generate pigmented cells. We noticed that the *h2a.z.2* mutant animals demonstrated comparable fin growth; however, they displayed decreased melanocyte regeneration kinetics (Fig. 6E,F). The level of achieved repigmentation is in tune with the severity of the ventral stripe pigmentation observed in these mutants (Fig. 6G). The NCC-derived fate-specified progenitors established in the skin and responded to melanocyte loss by providing requisite melanocytes. The decreased recall of melanocytes indicated that the progenitors were inadequately populated, and endorsed the role of *h2a.z.2* in melanocyte fate specification. Therefore, using targeted genome engineering, we unequivocally demonstrated the role of H2A.Z.2 in establishing a melanocyte progenitor population, which was evident not only at the embryonic stage but also during adult melanocyte regeneration.

## DISCUSSION

The decoding of cell fate decisions has emerged as an intense area of research, primarily because of the immense application potential it has in futuristic regenerative interventions. Fate establishment is perceived to be a continuum, wherein progressive fate bias culminates in determination and is controlled by appropriate external signals. Currently, we understand deterministic events better because of the characteristic gene expression signatures orchestrated by key TFs. However, the underlying molecular mechanisms behind the fate-biasing of specification events remains unexplored. The nondeterministic nature of fate bias induced during specification necessitates a modulatory role for the specifier for which epigenetic factors are perfectly suited. Histone modifications and the deposition of variants could function in conjunction with TFs and offer a greater plasticity to modulate the cell fate. A recent study identifies a selective role for H2A.Z.2 in craniofacial cartilage formation in *Xenopus* (Greenberg et al., 2019). Herein, the H2A.Z.2 variant is involved in this process but H2A.Z.1 is not. Our observations confirm the conservation of this function in zebrafish.

In this study, we establish the occupancy of H2A.Z.2 on the *mitf* promoter that facilitates its expression by upstream activating signals. We propose a model for melanocyte lineage specification, wherein H2A.Z.2 acts as a key specifying signal. Three of the fate-biasing transcriptional programmes in the neural crest lineage are involved in suppressing the melanocyte fate. These include *Sox2* (Adameyko et al., 2012) and *Neurog2* (Soldatov et al., 2019) from the neural lineage, and *Foxd3* (Ignatius et al., 2008; Kos et al., 2001) from the glial lineage, all of which actively suppress *Mitf* expression. In contrast, *H2a.z.2* is a positive regulator that promotes melanocyte fate bias, as its overexpression facilitates *Mitf* induction. A hierarchical fate-biasing model necessitates such opposing programmes to ensure defined populations of emerging differentiated cells. The observed concomitant decrease in the glial population suggests that H2A.Z.2 could operate as a specifier at the tripotent melanocyte/glial/neural progenitor level, driving the allocation towards a melanocyte-glial bipotent fate. The regulation of *Sox9* by H2a.z.2 could have a dual role of promoting *Mitf* expression in melanocytes and also facilitating the glial-specific programmes (Cheung and Briscoe, 2003).

Regenerative melanocytes arise from NCC-derived stem cells that are positioned along the lateral line in close juxtaposition with dorsal root ganglia in zebrafish embryos (Dooley et al., 2013). In the adult zebrafish, precursor cells directly differentiate into mature melanocytes and also divide to yield additional lineage-restricted cells (Iyengar et al., 2015). In mammalian skin, this population resembles nerve-associated melanocyte precursors (Adameyko et al., 2009) and the hair follicle bulge region progenitors that give rise to melanocytes at every hair cycle (Nishimura et al., 2002). These progenitors are thought to restore epidermal pigmentation after wound healing and during melanocyte regeneration in conditions such as vitiligo (Chou et al., 2013).

The establishment of melanocyte stem cells is thought to occur independently of *Mitf* (Johnson et al., 2011). However, all the downstream events involved in melanocyte fate determination are orchestrated by this master regulator. Hence the ‘melanocyte specification factor’ is likely to function upstream of Mitf. The transient epigenetic memory conferred by the incorporation of H2A.Z.2 at the *Mitf* promoter would not only facilitate its expression upon external cues such as WNT ligands, it would also enable the retention of this memory in transiently amplifying cells. The *Mitf*-inducing Wnt-signalling pathway triggers melanocyte regeneration by possibly activating this H2A.Z.2 occupied state of the *Mitf* promoter. Therefore, the histone variant-based specification elucidated in our study enables the retention of plasticity, a hallmark of the specified state. The identification of such upstream specification mechanisms would enable futuristic regenerative therapeutic approaches from induced pluripotent cells, by employing a selective activation of lineage determinants.

## MATERIALS AND METHODS

### Ethics statement

Fish experiments were performed in strict accordance with the institutional animal ethics approval (IAEC) of the CSIR-Institute of Genomics and Integrative Biology (IGIB), India (Proposal No 45a). All efforts were made to minimize animal suffering.

### Zebrafish lines and maintenance

Zebrafish of the line ASWT were bred, raised and maintained at 28.5°C according to standard protocols (Westerfield, 2000) and were housed at the

Development (2020) 147, dev182576. doi:10.1242/dev.182576

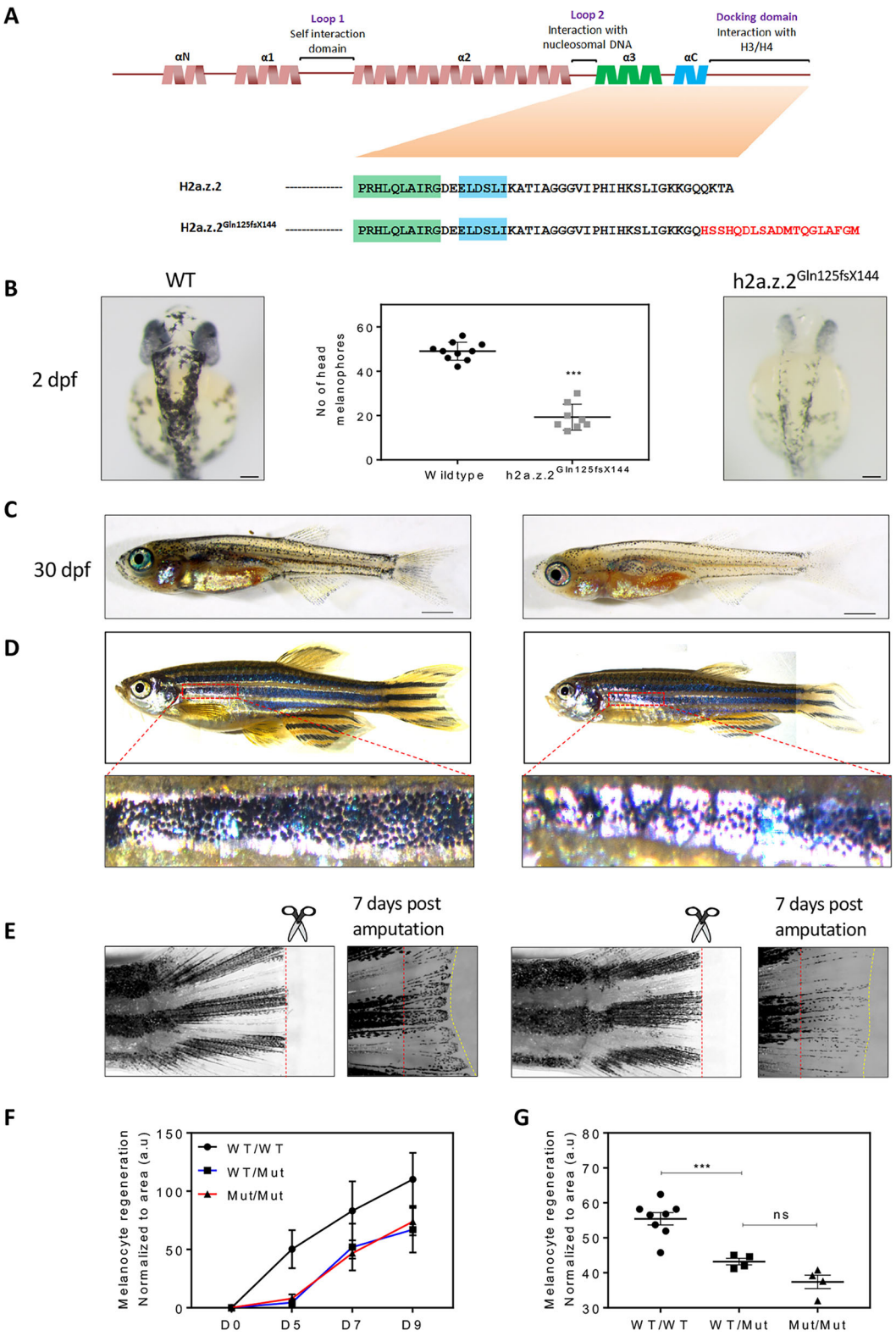


**Fig. 6. Targeted mutation of *h2a.z.2* affects melanocyte specification and regeneration.** (A) Top: orthology-based schematic of the secondary structure of zebrafish H2AZ.2. The functional elements in the protein are denoted above. Below: amino acid sequence in H2A.Z.2 and the CRISPR mutant (H2a.z.2$^{Gln125fsX144}$) generated in this study. (B) Representative images of wild-type and Z2 mutant embryos at 2 dpf. Right: wild-type sibling control. Left: homozygous H2a.z.2$^{Gln125fsX144}$ mutant embryo. Middle: quantification of head melanophore numbers. Scale bar: 100 µm. (C) Representative images of wild-type and Z2 mutant juveniles at 30 dpf. Scale bars: 1 mm. (D) Representative images of wild-type and Z2 mutant adult animals. Higher magnification images of the first ventral stripe are shown below. (Adult fishes were imaged in parts and stitched.) (E) Fin clip and regeneration images of adult wild-type and Z2 mutant animals. Red-dashed lines indicate the site of amputation and the yellow-dashed line indicates the margin of the regenerated fin. (F) Kinetics of melanophore pigment regeneration over a period of 9 days after fin amputation ($n$=4). (G) Quantification of melanophore pigment across wild-type (WT), homozygous and heterozygous H2a.z.2$^{Gln125fsX144}$ mutants upon regeneration.

Development (2020) 147, dev182576. doi:10.1242/dev.182576

CSIR-IGIB, Mathura Road New Delhi, India. Embryos were staged on the basis of time [hours post fertilization (hpf); days post fertilization (dpf)] and morphological features, according to Kimmel et al., 1995. Embryos older than 24 hpf were treated with 0.003% 1-phenyl-2-thiourea (PTU) to inhibit pigment formation, aiding fluorescent imaging and RNA *in situ* hybridization analysis, as and when experiments demanded the depigmentation of the animals. The plasmid *ftyrp1*:GFP was a kind gift from Dr Xiangyun Wei (University of Pennsylvania, USA) (Zou et al., 2006) and the construct was injected at a concentration of 10-20 pg along with 50-75 pg of Tol2 transposase mRNA into one-cell-stage zebrafish embryos to create the transgenic line at CSIR-IGIB. Founder lines were established and propagated, which showed an expression pattern similar to pt101 as reported by Zou et al. (2006). The details of the zebrafish lines used in this study are provided in Table S1.

### Single-cell data visualization

Single-cell transcriptomic data for 5 dpf zebrafish sox10+ cells was downloaded from GEO series GSE131136 (Saunders et al., 2019). The analysis was replicated as per their methods using Monocle v.2.99.1 (Qiu et al., 2017a,b; Trapnell et al., 2014) in RStudio v.3.6 (www.rstudio.com/) and the expression of h2afva (H2a.z.2) and h2afvb (H2a.z.1) in different cell types was plotted.

### MO injections

MOs for blocking translational initiation or splicing of RNA were designed by Gene Tools (Table S1). The minimum effective concentration was determined for each MO (Kaufman et al., 2016) using dosage titration experiments. Concentrations of various MOs used in this study as follows: 3-3.5 ng of *h2a.z.2* translation block (Z2 MO), 4-4.5 ng of *h2a.z.2* splice block (Z2 SB MO), 2 ng of *h2a.z.1* splice block (Z1 MO) (Sivasubbu et al., 2006) and 0.8 ng of double-targeting (*h2a.z.1* and *h2a.z.2*) translational block (Z1+Z2 MO). A standard control MO from Gene Tools, LLC was used as a control and dosed accordingly. The p53 MO was co-injected at a 1:1 ratio with the corresponding gene targeting MOs.

### Capped RNA injections

For rescue experiments, mouse *H2a.z.1* (Z1-RNA) and *H2a.z.2* (Z2-RNA) genes were amplified using primers listed in Table S1. Similarly, the zebrafish *mitfa* gene was amplified using PCR (Table S1) and cloned into the Zero Blunt TOPO vector (Thermo Scientific, K287540) according to the manufacturer's protocols. Capped and PolyA tail RNA was synthesized by *in vitro* transcription using the T7-Ultra mRNA Synthesis Kit (Thermo Scientific, AM1345) followed by PolyA tailing according to the manufacturer's protocol. A volume of 100 pg (for *H2a.z.1* and *H2a.z.2*) or 50 pg (for *mitfa*) was co-injected into one-cell-stage embryos along with the Z2 morpholino. Site-directed mutagenesis for mH2a.z.2 A14T, T38S and A127V was carried out using the SDM II kit (Agilent) using primers listed in Table S1 according to the manufacturer's protocols. Subsequently, the mutations were verified by Sanger sequencing and cloned into the Zero Blunt TOPO vector for capped and PolyA tail RNA synthesis.

### Whole-mount RNA *in situ* hybridization

RNA *in situ* hybridization was performed as described by Thisse and Thisse (2008). Riboprobes of the following genes were used for this study: *foxd3*, *sox10*, *crestin*, *krox20*, *sox9a* (Stewart et al., 2006), *mbp* (Brösamle and Halpern, 2002), *neuroD* (van der Velden et al., 2013), *isl2a* (Appel et al., 1995), *sox9b* (Yan et al., 2005), *tfap2a*, *mitfa*, *c-kit*, *dct* (Van Otterloo et al., 2010). Zebrafish *h2a.z.2* exon5-3′UTR (307 bp) was amplified using primers listed in Table S1. The product was subsequently cloned into pCR4-TOPO (Thermo Scientific, K287540) and was used as template for *in vitro* transcription of antisense probe using Megascript T7 (Thermo Scientific, AM1334).

### Imaging

Bright-field imaging for live imaging and gene expression pattern (WISH) studies of zebrafish embryos was performed using a Zeiss stereo microscope (Stemi 2000-C). A Zeiss Axioscope A1 Microscope (with AxiocamHRc) was used for fluorescence imaging. Zeiss proprietary software was used to capture images, which were processed and analysed in Adobe Photoshop CS3.

### Imaging flow cytometry-based population analysis

Cell counts for sox10:EGFP, mitfa:GFP, ftyrp1:GFP$^{+}$ cells and ASWT embryos (for melanophore counts) were performed using an AMNIS ImageStream MKII flow cytometer. Briefly, embryos were dechorinated using pronase (5 mg/ml) (Sigma-Aldrich, P8811) for 10-15 min and collected in microfuge tubes. The embryos were deyolked in ice cold Ringer's solution using a micropipette tip and spun at 100 ***g*** for 2 min in a tabletop centrifuge at 4°C (Eppendorf, 5418R). The supernatant was discarded and the embryo bodies were trypsinized using TrypLE Express (Thermo Scientific, 12604039) for 15 or 30 min for 24 hpf or 48 hpf, embryos respectively, at room temperature. The cell suspension was passed through a 70 µm cell strainer and washed twice with ice cold phosphate-buffered saline. The cell suspension was analysed in the imaging flow cytometry system and at least 50,000 images were captured and processed using IDEAS (AMNIS) software.

### Morphant *Tg(sox10: GFP)* cell sorting and microarray analysis

Control MO and Z2 MO were injected into one-cell-stage *Tg(sox10:GFP)* embryos and allowed to develop until 15 hpf. The embryos were processed in a similar manner as that for imaging flow cytometry analysis. Finally, the trypsinized cells were resuspended in ice cold PBS+10% fetal bovine serum and subjected to FACS (BD Biosciences FACSAria™ III). The GFP$^{+}$ cells were sorted and collected in RP1 buffer and RNA was isolated using Nucleospin RNA XS kit (Macherey Nagel, 740902) according to the manufacturer's protocol. The microarray experiment and subsequent analysis was outsourced to Genotypic Technology (Bengaluru, India).

### Cell line maintenance and culturing conditions

B16 mouse melanoma cells were cultured in DMEM-High glucose media (Sigma-Aldrich, D5648) supplemented with 10% FBS (Thermo Scientific) at 5% $CO_2$ (Eppendorf, New Brunswick Galaxy 170S incubator). Media was changed every day and cells were passaged upon reaching 80% confluence. Mouse R1 embryonic stem cells (R1/E) were cultured in DMEM Glutamax media supplemented with sodium pyruvate (Thermo Scientific,10569 010), MEM-NEAA (Thermo Scientific, 11140 050), 2-mercaptoethanol (Thermo Scientific, 31350 010) and 20% Pansera (Pan Biotech, P30 2602) at 5% $CO_2$. Media was changed every day and cells were passaged every other day.

### Melanocyte generation from R1/E mouse embryonic stem cells

Melanocytes were generated from R1/E mESCs using a modified protocol from Yang et al. (2011). For EB formation, cells were trypsinized and 50,000 cells/ml suspensions were prepared. Subsequently, 10 µl of this suspension was placed in the lid of a 90 mm Petri dish and inverted upon the base of the Petri dish filled with 15 ml of autoclaved MilliQ $H_2O$. After 4 days, the EBs were transferred to 24-well or 6-well plates coated with collagen (Thermo Scientific, A10483 01) containing melanocyte conversion media (45% DMEM – High glucose, 45% Reconstituted M254) (Thermo Scientific, M254CF), 10% FBS, 50 ng/ml SCF (Peprotech, 300 07 10), 100 nM Endothelin-3 (Sigma-Aldrich, E9137), 20 pM Cholera toxin (Sigma-Aldrich, C8052), 0.5 µM Dexamethasone (Sigma-Aldrich, D1756), 50 ng/ml WNT3a (Peprotech, 315 20 10), 4 ng/ml beta-FGF (Thermo Scientific, RFGFB50), 50 nM PMA (Sigma-Aldrich, P1585), 1 N2 Supplement (Thermo Scientific, 17502 048) and 1× Antibiotic-Antimycotic (Thermo Scientific, 15240 052). Cells were collected at specific time points for downstream analysis.

### Immunocytochemistry

Cells were plated on coverslips, washed twice with 0.01% Tween 20 in PBS, fixed with 4% paraformaldehyde for 10 min, permeabilized with 0.1% Triton X-100 in PBS for 10 min and washed three times with 0.01% Tween 20 in PBS. Coverslips were then incubated in blocking buffer (5% normal goat serum in 0.01% Tween 20) for 1 h followed by washing and overnight incubation with mouse anti-MITF (1:100, C-5, Abcam, ab12039) or rabbit anti-SOX10 (1:100, Abcam, ab155279) antibody at 4°C. This was followed by three washes with 0.01% Tween 20 and then incubation with Alexa Fluor

Development (2020) 147, dev182576. doi:10.1242/dev.182576

594 goat anti-mouse (for MITF) or anti-rabbit (for SOX10) dye for 1 h at room temperature. Coverslips were washed three times with 0.01% Tween 20 and then mounted in ProLong Gold Antifade Mountant with DAPI (Molecular Probes, Thermo Scientific). Images were visualized using a DeltaVision microscope (GE Healthcare).

### siRNA and plasmid transfections

$2\times10^5$ B16 melanoma cells were seeded in 6-well plates before the day of transfection. The following day, 100 nM of nontargeting control siRNA, *H2a.z.2* siRNA (siRNA pool of five siRNAs) (Dharmacon ON-TARGETplus; L-063612-01-0005) or *H2a.z.1* siRNA (siRNA pool of five siRNAs) (Dharmacon ON-TARGETplus; L-042994-01-0005) was transfected according to the manufacturer's protocol using Dharmafect (Dharmacon, T-2001) transfection reagent. Cells were collected at specified time points for downstream analysis. Plasmid transfections were performed using Lipofectamine 2000 (Thermo Scientific, 11668019).

### RNA isolation, cDNA synthesis and quantitative real-time PCR

RNA was isolated from zebrafish embryos,B16 melanoma cells or R1/E cells using Nucleospin Triprep (Macherey Nagel, 740966) according to the manufacturer's protocols. cDNA was synthesized using the Superscript III First-Strand cDNA Synthesis Kit (Thermo Scientific, 1800051). Quantitative real-time PCR was carried out as described (Pfaffl, 2001) using a Roche Lightcycler Real-Time PCR System. For quantification, the relative standard curve method was used (as described by the manufacturer) to generate raw values representing arbitrary units of RNA transcripts. Data analysis was performed using the $2^{-\Delta\Delta CT}$ method.

### shRNA transduction in R1/E ESCs

Lentiviral packaging and transduction was performed as previously reported by Motiani et al. (2018). Briefly, lentiviral packaging was performed by co-transfecting pVSVG, pdR8.2 and *H2a.z.2* shRNA, or nontargeting shRNA in HEK cells. Two days post-transfections, lentiviral particles were collected from the cell supernatant. Next, 1:100 HEPES pH 7.25 1 M stock solution and 1:100 Polybrene 0.4 mg/ml were added to the lentiviral supernatant. Embryonic stem cell media [ESCM; DMEM GlutaMax media supplemented with sodium pyruvate (Thermo Scientific; 11140-50), β-mercaptoethanol (Thermo Scientific; 31350-010) and 20% Pansera ES (Pan Biotech; P30-2602)] and lentiviral cocktail were mixed in a 1:1 ratio and added to R1/E ESCs. The mixture was spun for 30 min at 37°C and at 1076 ***g***. The cells were incubated at 37°C for 10-12 h and then the media was changed to fresh ESCM. Cells were checked for GFP fluorescence at 48 h after transduction in R1/E cells and were selected using 0.5 µg/ml puromycin for a week. Experiments were performed with FACS-sorted $GFP^+$ cells propagated as a pool.

### ChIP and qPCR

ChIP assays were performed according to the protocol provided by Upstate Biotechnology with modifications as suggested in the Fast ChIP protocol. The anti-H2A.Z antibody (Abcam, ab4174) was used for the assay. Anti-rabbit IgG (Thermo Scientific, 02-6102) was used for isotype control in all of the cell lines. Briefly, B16 melanoma cells or R1/E ESCs were fixed with 10% formalin (Sigma-Aldrich, HT501128) and incubated at 37°C for 10 min. Next, 2.5 M glycine (Sigma-Aldrich, 50046) was added to the cells and again incubated at 37°C for 10 min. Cells were washed with ice cold 1× PBS containing protease inhibitors. Cells were then scraped and centrifuged at 86 ***g*** for 5 min at 4°C. The cell pellet was lysed in SDS lysis buffer [1% SDS (Sigma-Aldrich, L3771), 10 mM EDTA (Sigma-Aldrich, E6758), 50 mM TRIS (Sigma-Aldrich, T6066) (pH 8.1)] on ice for 30 min. The cells were then sonicated in a Bioruptor (Diagenode) in ice. The chromatin lysate was then estimated for protein content using a BCA kit (Thermo Scientific, 23225). The samples were decrosslinked overnight at 65°C and deproteinized with Proteinase K (Sigma-Aldrich P4850). Sheared DNA was column-purified using a PCR Purification Kit (Qiagen, 28104) and estimated using a QUBIT dsDNA HS Kit (Thermo Scientific, Q32851). ChIP was performed using 3-5 µg of the respective antibody added to an equal amount of chromatin across samples and incubated overnight at 4°C (10% of chromatin was kept separately as input). Next day, 100 µl of Protein A agarose beads (G-Bioscience, 786 283) were added to the mixture of chromatin and antibody, and incubated for 4-6 h at 4°C. After incubation the beads were washed twice with low salt buffer [0.1% SDS, 1% Triton X-100 (Sigma-Aldrich, T8787), 2 mM EDTA, 20 mM Tris HCl (pH 8), 150 mM NaCl (Sigma-Aldrich, S3014)], high salt buffer [0.1% SDS, 1% Triton X-100, 2 mM EDTA, 20 mM Tris HCl (pH 8), 500 mM NaCl] and LiCl buffer [0.25 M LiCl (Sigma-Aldrich, D62476), 1% Igepal CA-630 (Sigma-Aldrich, I8896), 1 mM EDTA, 10 mM Tris HCl (pH 8), 1% deoxycholate (Sigma-Aldrich, D6750)]. Finally, the beads were washed with Tris EDTA buffer. The beads were then incubated with 100 µl elution buffer [1% SDS, 0.75% sodium bicarbonate (Sigma-Aldrich, S5761)] and 1 µl of 20 mg/ml proteinase K for 15 min; elution was performed again with 100 µl for another 15 min. Subsequently, the samples were kept for 12-14 h at 65°C for reverse crosslinking. After incubation, the samples were column-purified using the PCR Purification Kit; the inputs from each of the samples were also included in the purification step. SYBR green- (Kapa Biosystems) based qRT-PCR was set up using eluted DNA and graphs were plotted as percentage input. Primer sequences for target genes are provided in Table S1.

### Histone extraction from zebrafish embryos

Zebrafish embryos were dechorinated, deyolked and made into a single-cell suspension. Cell lysis was performed by adding 1 ml hypotonic lysis buffer to the cell pellet and gently mixing by pipetting to dissolve the cell pellet. The cells were incubated on a rotator at 4°C for 30 min and then centrifuged at 10,000 ***g*** for 10 min at 4°C. Nuclear lysis was performed by removing the supernatant and 400 µl of 0.4 N $H_2SO_4$ was added to the cells. The pellet was dissolved without any clumps and incubated at 4°C in a rotator overnight at 10 rpm. The samples were then centrifuged at 16,000 ***g*** for 10 min at 4°C. The supernatant containing histones was transferred to a fresh epitube. Histone precipitation was performed by adding TCA (trichloroacetic acid) (stock 66%; final concentration 33%) drop by drop to the tube while vortexing constantly at slow speed. The sample was then incubated on ice for 30 min until the solution turned milky white. The samples were centrifuged at 16,000 ***g*** for 10 min at 4°C. The supernatant was removed and the pellet was washed with 500 µl of ice cold acetone. The samples were centrifuged again at 16,000 ***g*** for 5 min at 4°C. The acetone wash step was repeated again. The pellet was air dried and then dissolved in nuclease-free water. Histone quantification was performed by running 10 µl of samples on a 12% SDS gel and stained with Coommassie Brilliant Blue R-250 overnight. The gel was scanned after destaining and densitometry was performed using ImageJ software. According to the ImageJ analysis, the sample volumes were recalculated for equal loading to perform western blotting.

### Luciferase assay

Mouse *mitf*-luciferase (a kind gift from Dr Krishnamurthy Natarajan, Jawaharal Nehru University, India) and *sox9*-luciferase (a kind gift from Dr Peter Koopman, The University of Queensland, Australia) constructs were co-transfected (at a ratio of 1:10) with *Renilla* luciferase (pRL-TK vector, Promega) into nontargeting control- or *H2a.z.2* siRNA-treated B16 melanoma cells, and B16 cells transfected with pIRES empty vector or pIRES-mH2a.z.2 vector. After 24 h the cells were lysed with passive lysis buffer and luciferase assays were performed according to the manufacturer's protocols (Dual Luciferase Reporter Assay System; Promega). Alpha MSH (Sigma-Aldrich, M4135) treatment was provided 6 h post-transfection of the luciferase constructs. Stable B16 cells containing the *Mitf* promoter luciferase were generated by transfecting the construct followed by selection with G418 for a week. This chromatinized reporter line was subsequently used for downstream experiments.

### CRISPR-based mutagenesis

sgRNA targeting the zebrafish *h2a.z.2* gene was selected using the ECRISP (www.e-crisp.org/E-CRISP/) online tool using default parameters. Primers were designed for generating the complete sgRNA (related to STAR methods: oligonucleotides) using annealing PCR. *In vitro* transcription was

performed on these PCR products using T7 MEGAshortscript Transcription Kit (Thermo Scientific) according to the manufacturer's protocols. Next, 100 pg of sgRNA was injected along with 500 pg of spCAS9 protein (kind gift from Dr Debojyoti Chakraborty, CSIR-IGIB, India). The F0 embryos were grown to adulthood and were then outcrossed with ASWT to give rise to F1 animals. In the F1 generation, genomic DNA was isolated from fin clips of putative mutants and the target region was amplified using primers provided (related to STAR methods: oligonucleotides). The PCR products were subjected to Sanger sequencing to confirm mutations.

We used the F2 generation h2a.z.2 mutants, namely h2a.z.2$^{Gln125fsX144}$, for this study. In the H2a.z.2$^{Gln125fsX144}$ mutants we observed a 10-base deletion in exon 5, which leads to skipping of the stop codon and adds an additional 14 amino acids to the H2a.z.2 protein sequence.

### Melanocyte regeneration via fin amputation

Fin amputation experiments were performed on heterozygous F1 mutant animals. Mature zebrafish adults (5-10 months) were anaesthetized and the distal two-thirds of the caudal fin was amputated with a scalpel. The amputated fin was imaged immediately using a stereozoom microscope (Zeiss Stemi 2000-C). The fish were then returned to fresh water at 25°C on a regular feeding schedule for the duration of the experiment. The fin was allowed to regenerate for a week, during which the quiescent melanocyte stem cells are stimulated and undergo the process of differentiation to generate pigmented cells. The tail fin of the fish was imaged again after 7 days and melanocyte regeneration was assessed.

### Statistical analysis and graphs

A Student's *t*-test was performed to determine statistical significance of the data. Asterisks on the error bars correspond to *$P \leq 0.05$, **$P \leq 0.01$, ***$P \leq 0.001$, ****$P \leq 0.0001$ and ns (not significant; $P > 0.05$). Graphs were plotted using GraphPad Prism.

#### Acknowledgements

We acknowledge Dr C. Sachidanandan (CSIR-IGIB, New Delhi, India) for providing several zebrafish lines and WISH probes; and B. Sharma for assistance with WISH experiments. We acknowledge the Imaging and FACS facility of CSIR-IGIB.

#### Competing interests

R.S.G. is the co-founder of the board of Vyome Biosciences Pvt Ltd, a biopharmaceutical company in the area of dermatology unrelated to the work presented here. The other authors declare no competing or financial interests.

#### Author contributions

Conceptualization: D.A.R., S.S., R.S.G., V.T.N.; Methodology: D.A.R., Y.S., A.A., V.G., A.B., J.T., R.K.M., S.S., V.T.N.; Validation: D.A.R., A.B., V.T.N.; Formal analysis: D.A.R., Y.S., A.A., V.G., R.S.G., V.T.N.; Investigation: D.A.R., Y.S., A.A., V.G., A.B., J.T., S.S., V.T.N.; Resources: S.S., V.T.N.; Data curation: V.T.N.; Writing - original draft: D.A.R., Y.S., V.G., V.T.N.; Writing - review & editing: D.A.R., R.S.G., V.T.N.; Visualization: D.A.R., Y.S., A.A., A.B., V.G., V.T.N.; Supervision: S.S., R.S.G., V.T.N.; Project administration: V.T.N.; Funding acquisition: R.S.G., V.T.N.

#### Funding

This work was supported by Council for Scientific and Industrial Research (CSIR) grants (TOUCH-BSC0302 to R.S.G. and V.T.N.; GRAFT-MLP1810 to V.T.N.), a CSIR-Young Scientist award (OLP1118 to V.T.N.), and the Department of Biotechnology, Ministry of Science and Technology (GAP0182 to V.T.N.). D.A.R. acknowledges their senior research fellowship from ICMR, India.

#### Data availability

Microarray data of isolated sox10 positive cells have been deposited in Gene Expression Omnibus under accession number GSE133141.

#### Supplementary information

Supplementary information available online at
http://dev.biologists.org/lookup/doi/10.1242/dev.182576.supplemental

#### References

**Adameyko, I., Lallemend, F., Aquino, J. B., Pereira, J. A., Topilko, P., Müller, T., Fritz, N., Beljajeva, A., Mochii, M., Liste, I. et al.** (2009). Schwann cell precursors from nerve innervation are a cellular origin of melanocytes in skin. *Cell* **139**, 366-379. doi:10.1016/j.cell.2009.07.049

**Adameyko, I., Lallemend, F., Furlan, A., Zinin, N., Aranda, S., Kitambi, S. S., Blanchart, A., Favaro, R., Nicolis, S., Lubke, M. et al.** (2012). Sox2 and Mitf cross-regulatory interactions consolidate progenitor and melanocyte lineages in the cranial neural crest. *Development* **139**, 397-410. doi:10.1242/dev.065581

**Appel, B., Korzh, V., Glasgow, E., Thor, S., Edlund, T., Dawid, I. B. and Eisen, J. S.** (1995). Motoneuron fate specification revealed by patterned LIM homeobox gene expression in embryonic zebrafish. *Development* **121**, 4117-4125.

**Bargaje, R., Alam, M. P., Patowary, A., Sarkar, M., Ali, T., Gupta, S., Garg, M., Singh, M., Purkanti, R., Scaria, V. et al.** (2012). Proximity of H2A.Z containing nucleosome to the transcription start site influences gene expression levels in the mammalian liver and brain. *Nucleic Acids Res.* **40**, 8965-8978. doi:10.1093/nar/gks665

**Bönisch, C., Schneider, K., Pünzeler, S., Wiedemann, S. M., Bielmeier, C., Bocola, M., Eberl, H. C., Kuegel, W., Neumann, J., Kremmer, E. et al.** (2012). H2A.Z.2.2 is an alternatively spliced histone H2A.Z variant that causes severe nucleosome destabilization. *Nucleic Acids Res.* **40**, 5951-5964. doi:10.1093/nar/gks267

**Brösamle, C. and Halpern, M. E.** (2002). Characterization of myelination in the developing zebrafish. *Glia* **39**, 47-57. doi:10.1002/glia.10088

**Cheung, M. and Briscoe, J.** (2003). Neural crest development is regulated by the transcription factor Sox9. *Development* **130**, 5681-5693. doi:10.1242/dev.00808

**Chou, W. C., Takeo, M., Rabbani, P., Hu, H., Lee, W., Chung, Y. R., Carucci, J., Overbeek, P. and Ito, M.** (2013). Direct migration of follicular melanocyte stem cells to the epidermis after wounding or UVB irradiation is dependent on Mc1r signaling. *Nat. Med.* **19**, 924-929. doi:10.1038/nm.3194

**Cox, S. G., Kim, H., Garnett, A. T., Medeiros, D. M., An, W. and Crump, J. G.** (2012). An essential role of variant histone H3.3 for ectomesenchyme potential of the cranial neural crest. *PLoS Genet.* **8**, e1002938. doi:10.1371/journal.pgen.1002938

**Curran, K., Lister, J. A., Kunkel, G. R., Prendergast, A., Parichy, D. M. and Raible, D. W.** (2010). Interplay between Foxd3 and Mitf regulates cell fate plasticity in the zebrafish neural crest. *Dev. Biol.* **344**, 107-118. doi:10.1016/j.ydbio.2010.04.023

**Dai, X., Bai, Y., Zhao, L., Dou, X., Liu, Y., Wang, L., Li, Y., Li, W., Hui, Y., Huang, X. et al.** (2017). H2A.Z represses gene expression by modulating promoter nucleosome structure and enhancer histone modifications in arabidopsis. *Mol. Plant* **10**, 1274-1292. doi:10.1016/j.molp.2017.09.007

**Donoghue, P. C. J., Graham, A. and Kelsh, R. N.** (2008). The origin and evolution of the neural crest. *BioEssays* **30**, 530-541. doi:10.1002/bies.20767

**Dooley, C. M., Mongera, A., Walderich, B. and Nusslein-Volhard, C.** (2013). On the embryonic origin of adult melanophores: the role of ErbB and Kit signalling in establishing melanophore stem cells in zebrafish. *Development* **140**, 1003-1013. doi:10.1242/dev.087007

**Dryhurst, D., Ishibashi, T., Rose, K. L., Eirín-López, J. M., McDonald, D., Silva-Moreno, B., Veldhoen, N., Helbing, C. C., Hendzel, M. J., Shabanowitz, J. et al.** (2009). Characterization of the histone H2A.Z-1 and H2A.Z-2 isoforms in vertebrates. *BMC Biol.* **7**, 86. doi:10.1186/1741-7007-7-86

**Dunn, K. J., Williams, B. O., Li, Y. and Pavan, W. J.** (2000). Neural crest-directed gene transfer demonstrates Wnt1 role in melanocyte expansion and differentiation during mouse development. *Proc. Natl. Acad. Sci. USA* **97**, 10050-10055. doi:10.1073/pnas.97.18.10050

**Faast, R., Thonglairoam, V., Schulz, T. C., Beall, J., Wells, J. R. E., Taylor, H., Matthaei, K., Rathjen, P. D., Tremethick, D. J. and Lyons, I.** (2001). Histone variant H2A.Z is required for early mammalian development. *Curr. Biol.* **11**, 1183-1187. doi:10.1016/S0960-9822(01)00329-3

**Gevry, N., Hardy, S., Jacques, P.-E., Laflamme, L., Svotelis, A., Robert, F. and Gaudreau, L.** (2009). Histone H2A.Z is essential for estrogen receptor signaling. *Genes Dev.* **23**, 1522-1533. doi:10.1101/gad.1787109

**Goding, C. R.** (2000). Mitf from neural crest to melanoma: signal transduction and transcription in the melanocyte lineage. *Genes Dev.* **14**, 1712-1728.

**Goding, C. and Meyskens, F. L., Jr.** (2006). Microphthalmic-associated transcription factor integrates melanocyte biology and melanoma progression. *Clin. Cancer Res.* **12**, 1069-1073. doi:10.1158/1078-0432.CCR-05-2648

**Greenberg, R. S., Long, H. K., Swigut, T. and Wysocka, J.** (2019). Single amino acid change underlies distinct roles of H2A.Z subtypes in human syndrome. *Cell* **178**, 1421-1436.e1424. doi:10.1016/j.cell.2019.08.002

**Hardy, S., Jacques, P.-E., Gévry, N., Forest, A., Fortin, M.-E., Laflamme, L., Gaudreau, L. and Robert, F.** (2009). The euchromatic and heterochromatic landscapes are shaped by antagonizing effects of transcription on H2A.Z deposition. *PLoS Genet.* **5**, e1000687. doi:10.1371/journal.pgen.1000687

**Hu, G., Cui, K., Northrup, D., Liu, C., Wang, C., Tang, Q., Ge, K., Levens, D., Crane-Robinson, C. and Zhao, K.** (2013). H2A.Z facilitates access of active and repressive complexes to chromatin in embryonic stem cell self-renewal and differentiation. *Cell Stem Cell* **12**, 180-192. doi:10.1016/j.stem.2012.11.003

**Hultman, K. A., Budi, E. H., Teasley, D. C., Gottlieb, A. Y., Parichy, D. M. and Johnson, S. L.** (2009). Defects in ErbB-dependent establishment of adult melanocyte stem cells reveal independent origins for embryonic and regeneration melanocytes. *PLoS Genet.* **5**, e1000544. doi:10.1371/journal.pgen.1000544

**Ignatius, M. S., Moose, H. E., El-Hodiri, H. M. and Henion, P. D.** (2008). colgate/hdac1 Repression of foxd3 expression is required to permit mitfa-dependent melanogenesis. *Dev. Biol.* **313**, 568-583. doi:10.1016/j.ydbio.2007.10.045

**Ignatius, M. S., Unal Eroglu, A., Malireddy, S., Gallagher, G., Nambiar, R. M. and Henion, P. D.** (2013). Distinct functional and temporal requirements for zebrafish Hdac1 during neural crest-derived craniofacial and peripheral neuron development. *PLoS ONE* **8**, e63218. doi:10.1371/journal.pone.0063218

**Iyengar, S., Kasheta, M. and Ceol, C. J.** (2015). Poised regeneration of zebrafish melanocytes involves direct differentiation and concurrent replenishment of tissue-resident progenitor cells. *Dev. Cell* **33**, 631-643. doi:10.1016/j.devcel.2015.04.025

**Jin, E.-J., Erickson, C. A., Takada, S. and Burrus, L. W.** (2001). Wnt and BMP signaling govern lineage segregation of melanocytes in the avian embryo. *Dev. Biol.* **233**, 22-37. doi:10.1006/dbio.2001.0222

**Johnson, S. L., Nguyen, A. T. N. and Lister, J. A.** (2011). mitfa is required at multiple stages of melanocyte differentiation but not to establish the melanocyte stem cell. *Dev. Biol.* **350**, 405-413. doi:10.1016/j.ydbio.2010.12.004

**Kaufman, C. K., Mosimann, C., Fan, Z. P., Yang, S., Thomas, A. J., Ablain, J., Tan, J. L., Fogley, R. D., van Rooijen, E., Hagedorn, E. J. et al.** (2016). A zebrafish melanoma model reveals emergence of neural crest identity during melanoma initiation. *Science* **351**, aad2197. doi:10.1126/science.aad2197

**Kawakami, A. and Fisher, D. E.** (2011). Key discoveries in melanocyte development. *J. Invest. Dermatol.* **131**, E2-E4. doi:10.1038/skinbio.2011.2

**Kawakami, A. and Fisher, D. E.** (2017). The master role of microphthalmia-associated transcription factor in melanocyte and melanoma biology. *Lab. Investig.* **97**, 649-656. doi:10.1038/labinvest.2017.9

**Kimmel, C. B., Ballard, W. W., Kimmel, S. R., Ullmann, B. and Schilling, T. F.** (1995). Stages of embryonic development of the zebrafish. *Dev. Dyn.* **203**, 253-310. doi:10.1002/aja.1002030302

**Kos, R., Reedy, M. V., Johnson, R. L. and Erickson, C. A.** (2001). The winged-helix transcription factor FoxD3 is important for establishing the neural crest lineage and repressing melanogenesis in avian embryos. *Development* **128**, 1467-1479.

**Le Douarin, N. M. and Dupin, E.** (2003). Multipotentiality of the neural crest. *Curr. Opin. Genet. Dev.* **13**, 529-536. doi:10.1016/j.gde.2003.08.002

**Le Douarin, N. M., Creuzet, S., Couly, G. and Dupin, E.** (2004). Neural crest cell plasticity and its limits. *Development* **131**, 4637-4650. doi:10.1242/dev.01350

**Lister, J. A., Robertson, C. P., Lepage, T., Johnson, S. L. and Raible, D. W.** (1999). nacre encodes a zebrafish microphthalmia-related protein that regulates neural-crest-derived pigment cell fate. *Development* **126**, 3757-3767.

**Madakashira, B., Corbett, L., Zhang, C., Paoli, P., Casement, J. W., Mann, J., Sadler, K. C. and Mann, D. A.** (2017). Variant Histone H2afv reprograms DNA methylation during early zebrafish development. *Epigenetics* **12**, 811-824. doi:10.1080/15592294.2017.1359382

**Marathe, H. G., Watkins-Chow, D. E., Weider, M., Hoffmann, A., Mehta, G., Trivedi, A., Aras, S., Basuroy, T., Mehrotra, A., Bennett, D. C. et al.** (2017). BRG1 interacts with SOX10 to establish the melanocyte lineage and to promote differentiation. *Nucleic Acids Res.* **45**, 6442-6458. doi:10.1093/nar/gkx259

**Martik, M. L. and Bronner, M. E.** (2017). Regulatory logic underlying diversification of the neural crest. *Trends Genet.* **33**, 715-727. doi:10.1016/j.tig.2017.07.015

**Matsuda, R., Hori, T., Kitamura, H., Takeuchi, K., Fukagawa, T. and Harata, M.** (2010). Identification and characterization of the two isoforms of the vertebrate H2A.Z histone variant. *Nucleic Acids Res.* **38**, 4263-4273. doi:10.1093/nar/gkq171

**Motiani, R. K., Tanwar, J., Raja, D. A., Vashisht, A., Khanna, S., Sharma, S., Srivastava, S., Sivasubbu, S., Natarajan, V. T. and Gokhale, R. S.** (2018). STIM1 activation of adenylyl cyclase 6 connects $Ca^{2+}$ and cAMP signaling during melanogenesis. *EMBO J.* **37**, e97597. doi:10.15252/embj.201797597

**Murphy, P. J., Wu, S. F., James, C. R., Wike, C. L. and Cairns, B. R.** (2018). Placeholder nucleosomes underlie germline-to-embryo DNA methylation reprogramming. *Cell* **172**, 993-1006.e1013. doi:10.1016/j.cell.2018.01.022

**Nishimura, E. K., Jordan, S. A., Oshima, H., Yoshida, H., Osawa, M., Moriyama, M., Jackson, I. J., Barrandon, Y., Miyachi, Y. and Nishikawa, S.-I.** (2002). Dominant role of the niche in melanocyte stem-cell fate determination. *Nature* **416**, 854-860. doi:10.1038/416854a

**Passeron, T., Valencia, J. C., Bertolotto, C., Hoashi, T., Le Pape, E., Takahashi, K., Ballotti, R. and Hearing, V. J.** (2007). SOX9 is a key player in ultraviolet B-induced melanocyte differentiation and pigmentation. *Proc. Natl. Acad. Sci. USA* **104**, 13984-13989. doi:10.1073/pnas.0705117104

**Pfaffl, M. W.** (2001). A new mathematical model for relative quantification in real-time RT-PCR. *Nucleic Acids Res.* **29**, e45. doi:10.1093/nar/29.9.e45

**Pünzeler, S., Link, S., Wagner, G., Keilhauer, E. C., Kronbeck, N., Spitzer, R. M. M., Leidescher, S., Markaki, Y., Mentele, E., Regnard, C. et al.** (2017). Multivalent binding of PWWP2A to H2A.Z regulates mitosis and neural crest differentiation. *EMBO J.* **36**, 2263-2279. doi:10.15252/embj.201695757

**Qiu, X., Hill, A., Packer, J., Lin, D., Ma, Y.-A. and Trapnell, C.** (2017a). Single-cell mRNA quantification and differential analysis with Census. *Nat. Methods* **14**, 309-315. doi:10.1038/nmeth.4150

**Qiu, X., Mao, Q., Tang, Y., Wang, L., Chawla, R., Pliner, H. A. and Trapnell, C.** (2017b). Reversed graph embedding resolves complex single-cell trajectories. *Nat. Methods* **14**, 979-982. doi:10.1038/nmeth.4402

**Rai, K., Jafri, I. F., Chidester, S., James, S. R., Karpf, A. R., Cairns, B. R. and Jones, D. A.** (2010). Dnmt3 and G9a cooperate for tissue-specific development in zebrafish. *J. Biol. Chem.* **285**, 4110-4121. doi:10.1074/jbc.M109.073676

**Raible, D. W. and Eisen, J. S.** (1994). Restriction of neural crest cell fate in the trunk of the embryonic zebrafish. *Development* **120**, 495-503.

**Saunders, L. M., Mishra, A. K., Aman, A. J., Lewis, V. M., Toomey, M. B., Packer, J. S., Qiu, X., McFaline-Figueroa, J. L., Corbo, J. C., Trapnell, C. et al.** (2019). Thyroid hormone regulates distinct paths to maturation in pigment cell lineages. *eLife* **8**, e45181. doi:10.7554/eLife.45181

**Sivasubbu, S., Balciunas, D., Davidson, A. E., Pickart, M. A., Hermanson, S. B., Wangensteen, K. J., Wolbrink, D. C. and Ekker, S. C.** (2006). Gene-breaking transposon mutagenesis reveals an essential role for histone H2afza in zebrafish larval development. *Mech. Dev.* **123**, 513-529. doi:10.1016/j.mod.2006.06.002

**Soldatov, R., Kaucka, M., Kastriti, M. E., Petersen, J., Chontorotzea, T., Englmaier, L., Akkuratova, N., Yang, Y., Haring, M., Dyachuk, V. et al.** (2019). Spatiotemporal structure of cell fate decisions in murine neural crest. *Science* **364**, 971-984. doi:10.1126/science.aas9536

**Stewart, R. A., Arduini, B. L., Berghmans, S., George, R. E., Kanki, J. P., Henion, P. D. and Look, A. T.** (2006). Zebrafish foxd3 is selectively required for neural crest specification, migration and survival. *Dev. Biol.* **292**, 174-188. doi:10.1016/j.ydbio.2005.12.035

**Takeda, K., Yasumoto, K.-I., Takada, R., Takada, S., Watanabe, K.-I., Udono, T., Saito, H., Takahashi, K. and Shibahara, S.** (2000). Induction of melanocyte-specific microphthalmia-associated transcription factor by Wnt-3a. *J. Biol. Chem.* **275**, 14013-14016. doi:10.1074/jbc.C000113200

**Thisse, C. and Thisse, B.** (2008). High-resolution in situ hybridization to whole-mount zebrafish embryos. *Nat. Protoc.* **3**, 59-69. doi:10.1038/nprot.2007.514

**Trapnell, C., Cacchiarelli, D., Grimsby, J., Pokharel, P., Li, S., Morse, M., Lennon, N. J., Livak, K. J., Mikkelsen, T. S. and Rinn, J. L.** (2014). The dynamics and regulators of cell fate decisions are revealed by pseudotemporal ordering of single cells. *Nat. Biotechnol.* **32**, 381-386. doi:10.1038/nbt.2859

**van der Velden, Y. U., Wang, L., Querol Cano, L. and Haramis, A.-P. G.** (2013). The polycomb group protein ring1b/rnf2 is specifically required for craniofacial development. *PLoS ONE* **8**, e73997. doi:10.1371/journal.pone.0073997

**Van Otterloo, E., Li, W., Bonde, G., Day, K. M., Hsu, M.-Y. and Cornell, R. A.** (2010). Differentiation of zebrafish melanophores depends on transcription factors AP2 alpha and AP2 epsilon. *PLoS Genet.* **6**, e1001122. doi:10.1371/journal.pgen.1001122

**Vardabasso, C., Gaspar-Maia, A., Hasson, D., Pünzeler, S., Valle-Garcia, D., Straub, T., Keilhauer, E. C., Strub, T., Dong, J., Panda, T. et al.** (2015). Histone variant H2A.Z.2 mediates proliferation and drug sensitivity of malignant melanoma. *Mol. Cell* **59**, 75-88. doi:10.1016/j.molcel.2015.05.009

**Wagner, D. E., Weinreb, C., Collins, Z. M., Briggs, J. A., Megason, S. G. and Klein, A. M.** (2018). Single-cell mapping of gene expression landscapes and lineage in the zebrafish embryo. *Science* **360**, 981-987. doi:10.1126/science.aar4362

**Watanabe, A., Takeda, K., Ploplis, B. and Tachibana, M.** (1998). Epistatic relationship between Waardenburg syndrome genes MITF and PAX3. *Nat. Genet.* **18**, 283-286. doi:10.1038/ng0398-283

**Westerfield, M.** (2000). *A Guide for the Laboratory use of Zebrafish (Danio rerio)*. Eugene: Univ. of Oregon Press.

**White, R. M. and Zon, L. I.** (2008). Melanocytes in development, regeneration, and cancer. *Cell Stem Cell* **3**, 242-252. doi:10.1016/j.stem.2008.08.005

**Yan, Y.-L., Willoughby, J., Liu, D., Crump, J. G., Wilson, C., Miller, C. T., Singer, A., Kimmel, C., Westerfield, M. and Postlethwait, J. H.** (2005). A pair of Sox: distinct and overlapping functions of zebrafish sox9 co-orthologs in craniofacial and pectoral fin development. *Development* **132**, 1069-1083. doi:10.1242/dev.01674

**Yang, R., Jiang, M., Kumar, S. M., Xu, T., Wang, F., Xiang, L. and Xu, X.** (2011). Generation of melanocytes from induced pluripotent stem cells. *J. Invest. Dermatol.* **131**, 2458-2466. doi:10.1038/jid.2011.242

**Zou, J., Beermann, F., Wang, J., Kawakami, K. and Wei, X.** (2006). The Fugu tyrp1 promoter directs specific GFP expression in zebrafish: tools to study the RPE and the neural crest-derived melanophores. *Pigm. Cell Res.* **19**, 615-627. doi:10.1111/j.1600-0749.2006.00349.x

**Zovkic, I. B., Paulukaitis, B. S., Day, J. J., Etikala, D. M. and Sweatt, J. D.** (2014). Histone H2A.Z subunit exchange controls consolidation of recent and remote memory. *Nature* **515**, 582-586. doi:10.1038/nature13707

# Supplementary figures

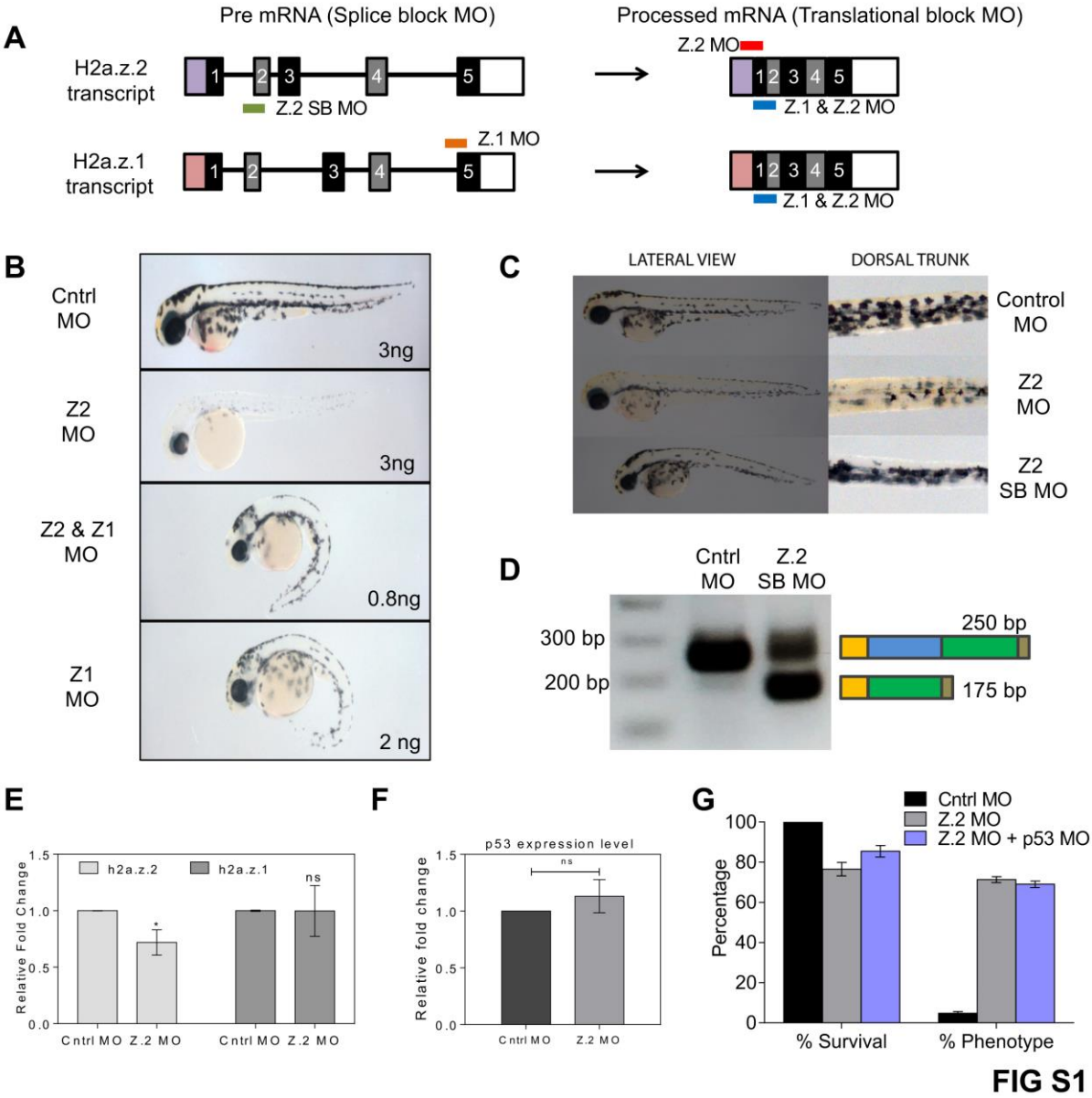


**Fig S1: Validating H2a.z.2 specific pigmentation phenotype using multiple silencing approaches**

(A) Schematic representing the target region for H2a.z.2 MO (Z2), H2a.z.1 MO (Z1), H2a.z.2 splice block (Z2 SB MO) and Z2 & Z1 MO.

(B) Brightfield images representing 48 hpf embryos injected with Control MO, Z2 MO, Z1 MO, Z1 & Z2 MO.

(C) Brightfield images showing lateral and dorsal view of Control MO, Z2 MO and Z2 SB MO embryos at 48 hpf.

(D) H2a.z.2 RT-PCR amplicons from control and Z2 SB MO injected embryos depicting the mis-spliced product.

(E) Bar graphs representing mRNA levels of h2a.z.1 and h2a.z.2 upon Z2 MO injection. Bars represent mean ± SEM across n=3 biological replicates.
(F) Bar graphs representing relative p53 mRNA levels in Z2 MO as compared to control MO. Bars represent mean ± SEM across n=5 biological replicates.
(G) Grouped bar plots representing percentage survival and pigmentation phenotype observed across control MO, Z2 MO and Z2 + p53 MO. Bars represent mean ± SEM across n=6 biological replicates.

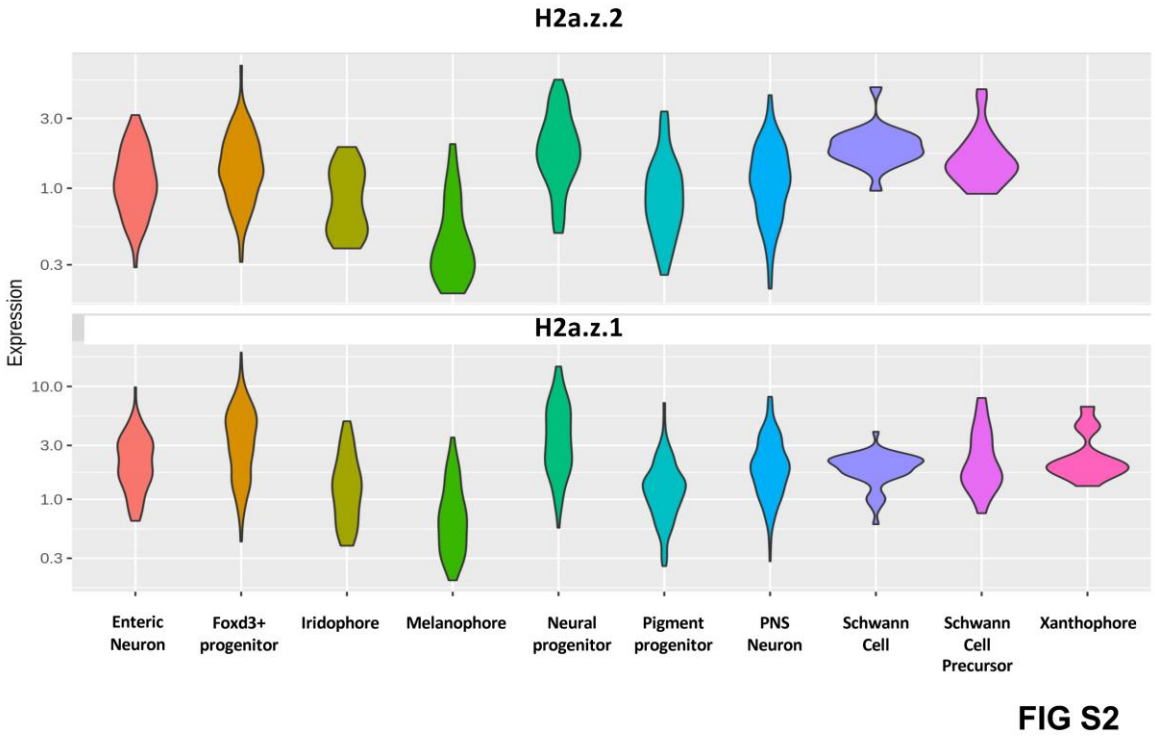


**Fig S2: Single cell meta-analysis of zebrafish sox10 positive cells and their derivatives.** Expression of H2a.z.2 (Adameyko et al.) and H2a.z.1 (bottom) from zebrafish single cell sequencing data (GSE131136), X-axis different cell types are indicated, Y-axis represents gene expression values in UMI counts.

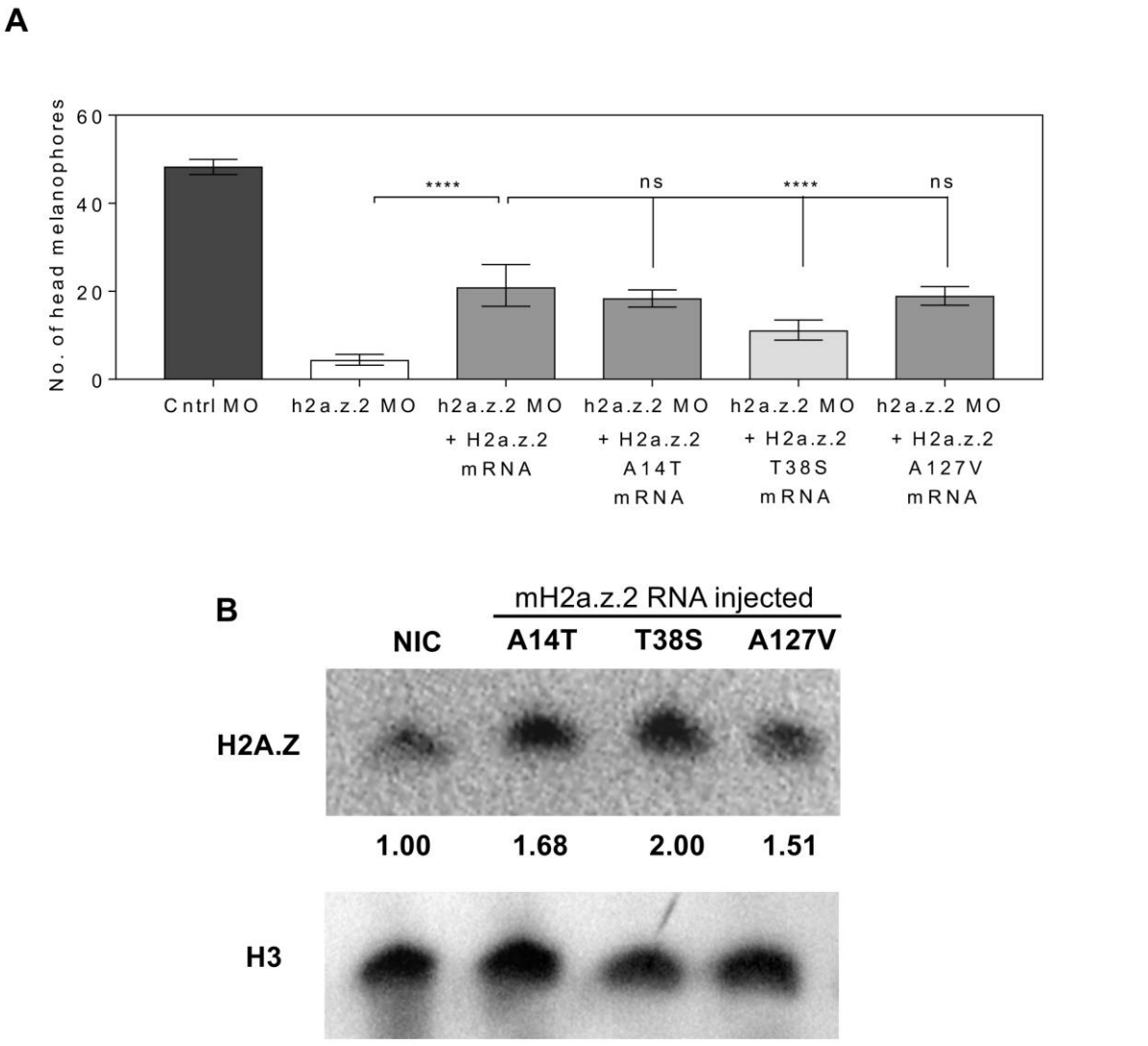


FIG S3

**Fig S3: A single amino acid substitution of T38S in mouse H2A.Z.2 contributes largely to the observed pigmentation effects**

(A) Bar graphs representing the number of head melanophores, denote geometric mean with 95% CI, representing data of n ≥ 50 embryos.

(B) Western blot analysis using H2AZ antibody in RNA injected embryos with H2a.z.2 mutants, normalised to H3. Numbers represent H3 normalized fold change compared to non-injected control (Adameyko et al.).

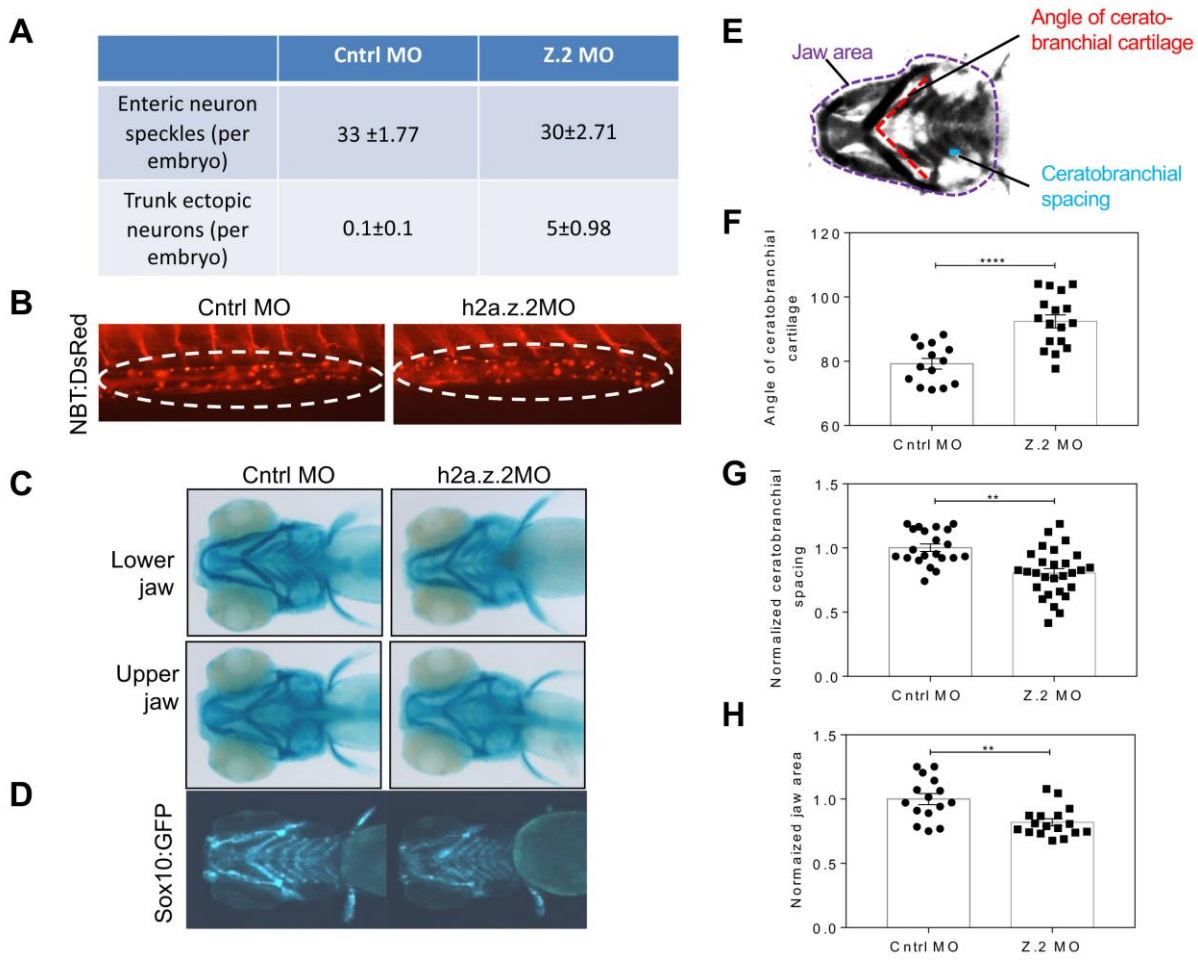


FIG S4

**Fig S4: Status of neural crest derivatives in H2a.z.2 morphants**

(A) Table enumerating the number of enteric, and trunk ectopic neurons observed in control and Z2 morphants. Numbers represent mean ± SD counted manually across ~50 embryos.

(B) Fluorescence images of enteric neurons in control and Z2 morphants in *Tg(NBT:DsRed)* fish embryos at 5 dpf.

(C) Alcian blue staining highlighting the craniofacial cartilage and fin cartilage in control and Z2 morphants.

(D) Fluorescence images of *Tg(sox10:EGFP)* head region representing the craniofacial cartilage system in control and Z2 morphants.

(E) Image representing the parameters utilized for jaw defect quantification in Z2 morphants represented in panels F to H.

(F) Bar graphs representing angle of the ceratobranchial cartilage in Z2 MO as compared to control. Bars represent mean ± SEM across $n \geq 15$ embryos.

(G) Bar graphs representing ceratobranchial spacing in Z2 MO as compared to control. Bars represent mean ± SEM across $n \geq 15$ embryos.

(H) Bar graphs representing area of the jaw in Z2 MO as compared to control. Bars represent mean ± SEM across $n \geq 15$ embryos.

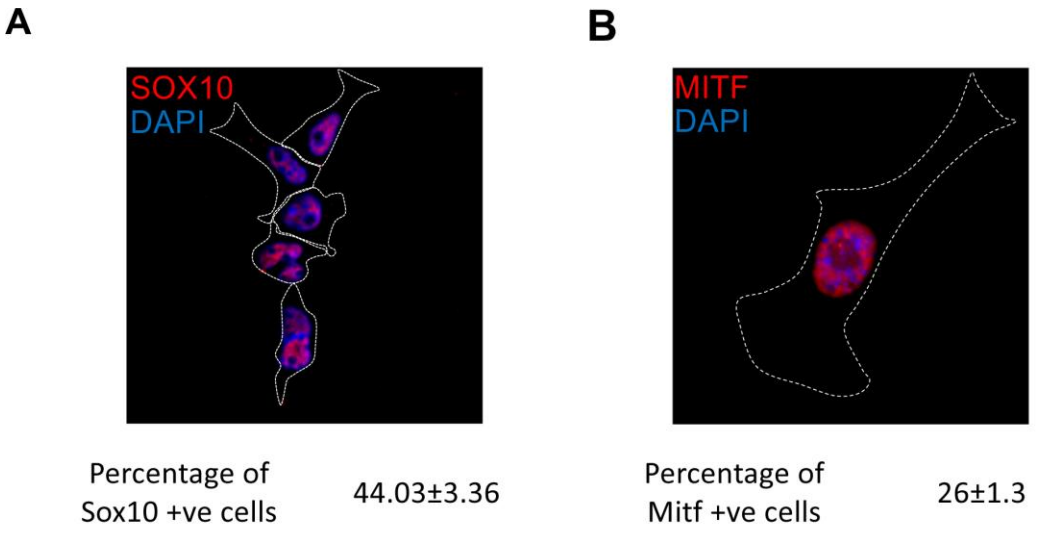


**Fig S5: R1E to melanocyte differentiation generates SOX10 and MITF positive cells**

(A) Immunocytochemistry for SOX10 counterstained with DAPI in Day10 after differentiation in melanocyte promoting medium.

(B) Immunocytochemistry for MITF counterstained with DAPI in Day10 differentiated cells.

Numbers at the bottom of the image represents percentage of cells positive for SOX10 and MITF staining respectively. At least 500 cells were taken for analysis.

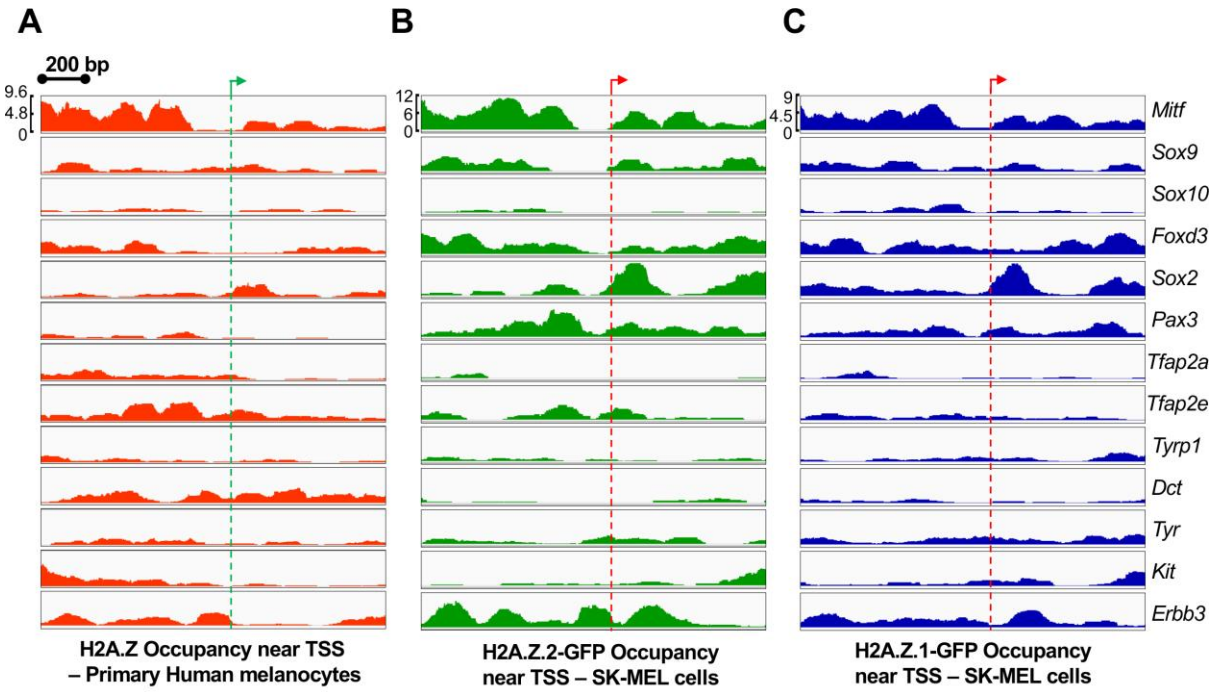


**Fig S6: H2A.Z occupancy in primary melanocytes and SKMEL cells**

(A-C) Metanalysis of chromatin immunoprecipitaton (ChIP) data in melanocyte derived lines from GSE68223.

(A) H2A.Z (Z1 + Z2) occupancy near transcription start site (TSS) in primary human melanocytes.

(B) H2A.Z.2-GFP occupancy near TSS in SK-Mel 147 metastatic melanoma cells.

(C) H2A.Z.1-GFP occupancy near TSS in SK-Mel 147 metastatic melanoma cells.

Dotted line indicates the TSS. Gene names are displayed on right corresponding to their ChIP seq profiles. Percent enrichment relative to input in the ChIP-seq data is displayed to the left for the top panel.

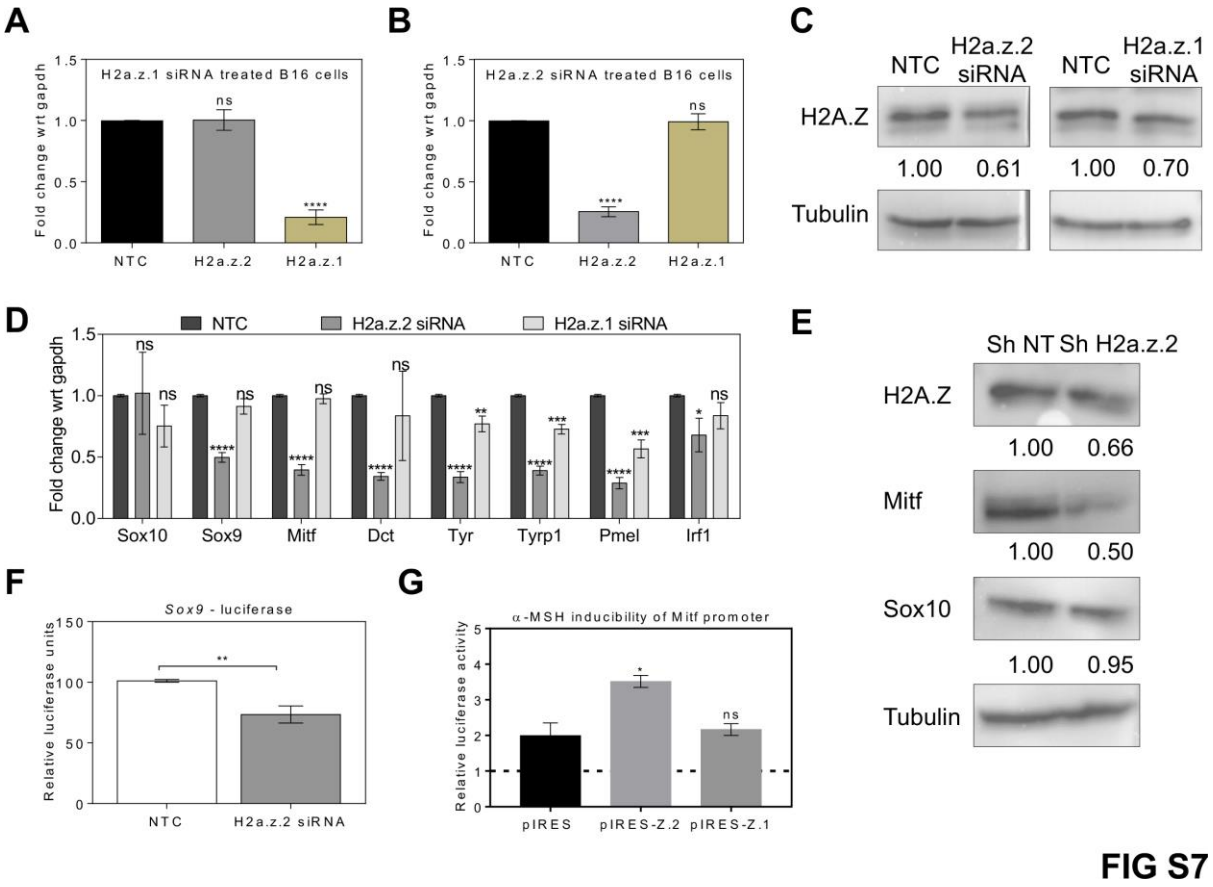


**FIG S7**

**Fig S7: H2A.Z mediates gene expression changes in B16 melanoma cells**

(A) Bar graph representing mRNA levels of *H2a.z.1* and *H2a.z.2* upon *Z1* silencing (mean ± SEM, n=3).

(B) Bar graph representing mRNA levels of *H2a.z.1* and *H2a.z.2* upon *Z2* silencing (mean ± SEM, n=3).

(C) Western blot analysis of total H2A.Z levels upon H2a.z.1 and H2a.z.2 siRNA treatment, normalized to tubulin.

(D) Bar plot representing relative mRNA levels of pigmentation related genes upon Z2 and Z1 silencing in B16 cells (mean ± SEM, n=3).

(E) Western blot analysis of total H2A.Z, MITF and SOX10 levels upon H2a.z.2 shRNA treatment in B16 melanoma cells, normalized to tubulin. Numbers represent tubulin normalized values with respect to shNT condition.

(F) Bar graphs representing the relative Sox9 luciferase activity of cells treated with non targeting control and Z2 siRNA (mean±SEM, N=4).

(G) Bar graphs representing the relative Mitf luciferase activity of B16 stable cells transfected with empty pIRES vector or pIRES containing H2a.z.1 or H2a.z.2 upon α-MSH treatment (mean ± SEM, n=4).

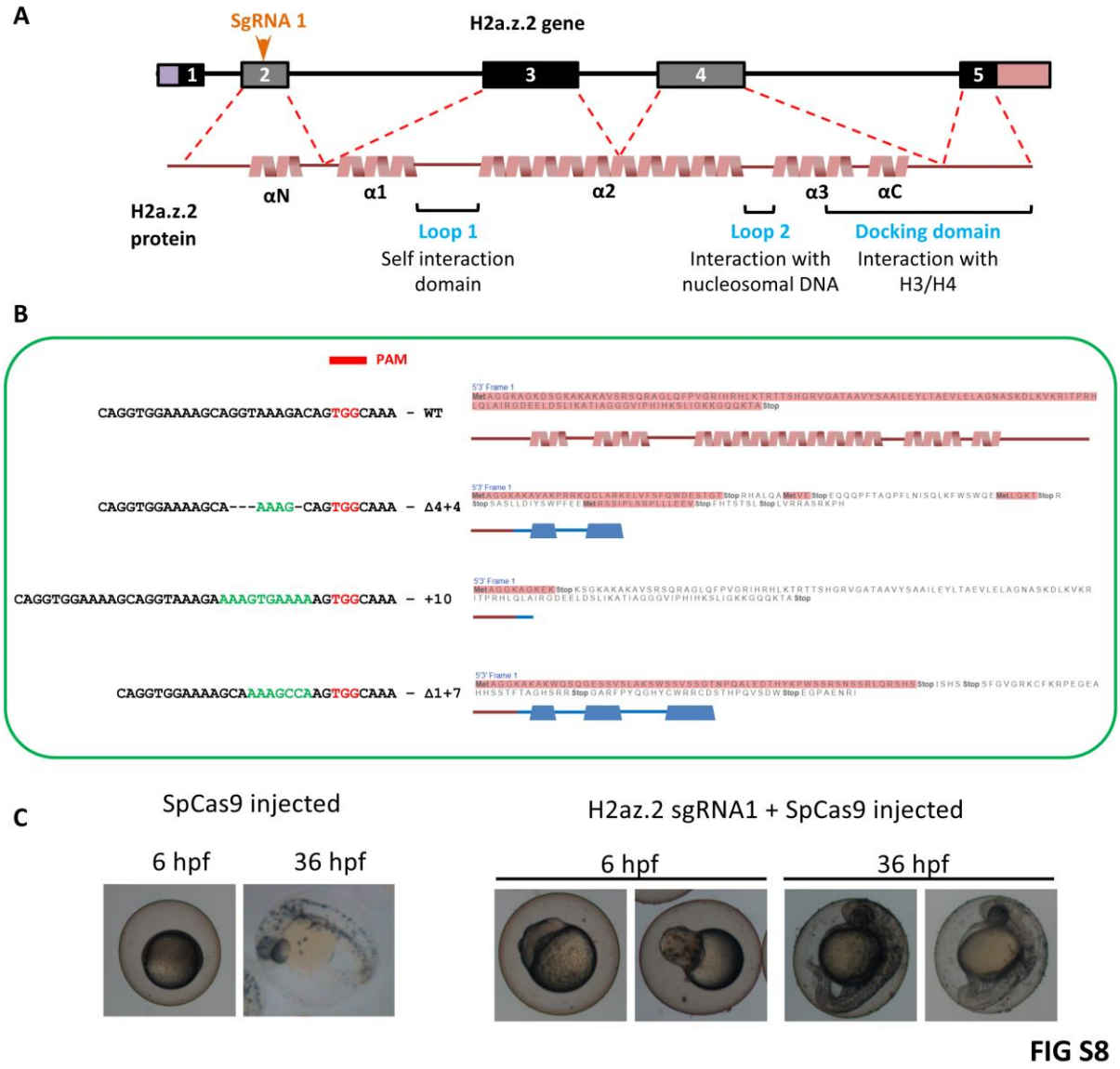


FIG S8

**Fig S8: CRISPR mediated targeting of *h2a.z.2* N-terminus region is lethal in zebrafish**

(A) Schematic representing the region targeted by *h2a.z.2* sgRNA1.

(B) Sequences displaying representative mutations occurred upon *h2a.z.2* sgRNA1 injections leading to embryonic lethality; predicted protein sequences are displayed on the right hand side.

(C) Bright field images of SpCas9 and SpCas9 + sgRNA1 injected embryos at 6 and 36 hpf.

**TABLE S1**

| REAGENT or RESOURCE | SOURCE | IDENTIFIER |
|---|---|---|
| **Antibodies** | | |
| Anti-Histone H2A.Z antibody | Abcam | Cat No: ab4174; RRID:AB_304345 |
| Anti-Histone H3 antibody | Abcam | Cat No:ab1791; RRID:AB_302613 |
| Anti-Beta tubulin antibody-HRP | Abcam | Cat No: ab21058; RRID:AB_727045 |
| Anti-MITF antibody | Abcam | Cat No: ab12039; RRID:AB_298801 |
| Anti-SOX10 antibody | Abcam | Cat No: ab155279; RRID:AB_2650603 |
| Anti-Digoxigenin-AP, Fab fragments from sheep | Sigma | Cat No: **11093274910** Roche ; RRID:AB_514497 |
| Anti-Rabbit IgG | Thermo Fisher Scientific | Cat No: 02-6102; RRID:AB_2532938 |
| Goat anti-Mouse IgG (H+L) Cross-Adsorbed ReadyProbes™ Secondary Antibody, Alexa Fluor 594, Thermo Fisher Scientific | Thermo Fisher Scientific | Cat No: R37121; RRID: AB_2556549 |
| Goat anti-Rabbit IgG (H+L) Cross-Adsorbed ReadyProbes™ Secondary Antibody, Alexa Fluor 594, Thermo Fisher Scientific | Thermo Fisher Scientific | Cat No: A-11037; RRID: AB_25344095 |
| | | |
| **Chemicals, Peptides, and Recombinant Proteins** | | |
| N-Phenylthiourea | Sigma | Cat No: P7629 |
| Pronase | Sigma | Cat No: P8811 |
| TrypLE Express | Thermo Fisher Scientific | Cat No: 12604039 |
| DMEM-High glucose media | Sigma | Cat No: D5648 |
| Fetal Bovine Serum | Thermo Fisher Scientific | Cat No: 10270-106 |
| DMEM-Glutamax supplemented with sodium pyruvate | Thermo Fisher Scientific | Cat No: 10569-010 |
| MEM-NEAA | Thermo Fisher Scientific | Cat No: 11140-050 |
| Beta-mercaptoethanol | Thermo Fisher Scientific | Cat No: 31350-010 |
| PANSERA | Pan Biotech | Cat No: P30-2602 |
| Collagen | Thermo Fisher Scientific | Cat No: A10483-01 |
| M254 | Thermo Fisher Scientific | Cat No: M254-CF |
| SCF | Peprotech | Cat No: 300-07-10 |

| | | |
|---|---|---|
| Endothelin-3 | Sigma | Cat No: E9137 |
| Cholera toxin | Sigma | Cat No: C8052 |
| Dexamethasone | Sigma | Cat No: D1756 |
| WNT-3a | Peprotech | Cat No: 315-20-10 |
| b-FGF | Thermo Fisher Scientific | Cat No: RFGFB50 |
| PMA | Sigma | Cat No: P1585 |
| N2-Supplement | Thermo Fisher Scientific | Cat No: 17502-048 |
| Anti-Anti | Thermo Fisher Scientific | Cat No: 15240-062 |
| Protein A agarose beads | G-Biosciences | Cat No: 786-283 |
| SYBR Green | KAPA biosystems | Cat No: KK4601 |
| Alpha-MSH | Sigma | Cat No: M4135 |
| | | |
| **Critical Commercial Assays** | | |
| Zero Blunt TOPO vector | Thermo Fisher Scientific | Cat No: K287540 |
| T7-ULTRA mRNA synthesis kit | Thermo Fisher Scientific | Cat No: AM1345 |
| Nucleospin RNA XS kit | Macherey Nagel | Cat No: 740902 |
| Non targeting control siRNA | Dharmacon ON-TARGETplus | Cat No: D-001810-10-05 |
| Mouse *H2a.z.2* siRNA | Dharmacon ON-TARGETplus | Cat No: L-063612-01-0005 |
| Mouse *H2a.z.1* siRNA | Dharmacon ON-TARGETplus | Cat No: L-042994-01-0005 |
| Dharmafect transfection reagent | Dhamacon | Cat No: T-2001 |
| Lipofectamine 2000 | Thermo Fisher Scientific | Cat No: 11668019 |
| Nucleospin Triprep | Macherey Nagel | Cat No: 740966 |
| Superscript III cDNA synthesis kit | Thermo Fisher Scientific | Cat No: 1800051 |
| GIPZ *H2a.z.2* shRNA | Dharmacon | Cat No: RMM4532-EG77605 |
| BCA Kit | Thermo Fisher Scientific | Cat No: 23225 |
| QUBIT ds HS DNA estimation kit | Thermo Fisher Scientific | Cat No: Q32851 |
| Dual luciferase assay system | Promega | Cat No: E1960 |
| T7 Megashortscript kit | Thermo Fisher Scientific | Cat No: AM1354 |
| | | |

| | | |
|---|---|---|
| **Deposited Data** | | |
| Raw and analyzed microarray data | This paper | GSE133141 |
| | | |
| **Experimental Models: Cell Lines** | | |
| B16 melanoma cell | | RRID: CVCL_0158 |
| ES-R1 cell line | | RRID: CVCL_2167 |
| | | |
| **Experimental Models: Organisms/Strains** | | |
| *ASWT* | Patowary A et al; 2013. | ZFIN ID: ZDB-PUB-130423-9 |
| *Tg(–4.9Sox10:egfp)$^{ba2}$* | Carney T J et al; 2006. | ZFIN ID: ZDB-ALT-050913-4 |
| *Tg(mitfa:GFP)$^{w47}$* | Curran K et al; 2009. | ZFIN ID: ZDB-ALT-081203-1 |
| *Tg(NBT-dsRed)* | Peri F et al; 2008. | ZFIN ID: ZDB-TGCONSTRCT-081023-2 |
| *Tg(foxd3:GFP)* | Gilnour DT et al; 2002 | ZFIN ID: ZDB-TGCONSTRCT-070117-95 |
| *Tg(ftyrp1:GFP)* | Zou J et al; 2006. | N/A |
| | | |
| **Oligonucleotides** | | |
| T7 promoter-Mouse H2a.z.1 CDS FP: TAATACGACTCACTATAGGGAGAGCA AACATGGCTGGCGGTAAGGC | This paper; Sigma | N/A |
| Mouse H2a.z.1 CDS RP: TTAAACAGTCTTCTGTTGTCCTTTC | This paper; Sigma | N/A |
| T7 promoter-Mouse H2a.z.2 CDS FP: TAATACGACTCACTATAGGGAGAGCA AACATGGCTGGAGGCAAAGCTG | This paper; Sigma | N/A |
| Mouse H2a.z.2 CDS RP: CTAAGCAGTTTTCTGCTGCCCC | This paper; Sigma | N/A |
| Zebrafish mitfa CDS FP: ATGTTGGAGATGCTCGAGTA | This paper; Sigma | N/A |
| Zebrafish mitfa CDS RP: CTAACAGCCATTGTCATGTT | This paper; Sigma | N/A |
| Zebrafish *h2a.z.2* WISH FP: GTGCAGACATGACTCAAGGACT | This paper; Sigma | N/A |
| Zebrafish *h2a.z.2* WISH RP: ATAAAACAGCTCCACGGCTC | This paper; Sigma | N/A |
| Z.2 Splice block check primer FP: ACCTCCCAGGATCCCATTCA | This paper; Sigma | N/A |
| Z.2 Splice block check primer RP: TGCCAACTCCAAAACTTCAGC | This paper; Sigma | N/A |
| Z.1 MO TGTGAGGAATGACTCCTGCGGACGC | Sivasubbu S et al; 2006 | N/A |

| | | |
|---|---|---|
| Z.2 MO<br>CCACCTGCCATTTCAGCGATGT | This paper;<br>Genetools | N/A |
| Z.1 – Z.2 MO<br>CTTTACCTGCTTTTCCACCTGCCAT | This paper;<br>Genetools | N/A |
| Z.2 Splice block MO<br>TCCACCTGCCTGCAAAACAATAATT | This paper;<br>Genetools | N/A |
| Control MO<br>CCTCTTACCTCAGTTACAATTTATA | Genetools | N/A |
| P53 MO<br>GCGCCATTGCTTTGCAAGAATTG | Genetools | N/A |
| Zebrafish *h2a.z.2* sgRNA 1<br>GGAAAAGCAGGTAAAGACAG | This paper;<br>Sigma | N/A |
| Zebrafish *h2a.z.2* sgRNA 2<br>GGGAGCTCCTCATCTCCTCGAA | This paper;<br>Sigma | N/A |
| Zebrafish *h2a.z.2* sgRNA 3<br>GGAGCTCGATTCCCTTATCA | This paper;<br>Sigma | N/A |
| Zebrafish *h2a.z.2* sgRNA 4<br>GGAACTATGCGGTTTTCTGC | This paper;<br>Sigma | N/A |
| Zebrafish *h2a.z.2* sgRNA 1<br>target region amplification FP<br>TGTTTGCTTGCATTGGATTGAGT | This paper;<br>Sigma | N/A |
| Zebrafish *h2a.z.2* sgRNA 1<br>target region amplification RP<br>CAGCTGTGAGATATTCAAGAATGG | This paper;<br>Sigma | N/A |
| Zebrafish *h2a.z.2* sgRNA 2&3<br>target region amplification FP<br>CATTGAAGCTGATATGGCAAACTT | This paper;<br>Sigma | N/A |
| Zebrafish *h2a.z.2* sgRNA 2&3<br>target region amplification RP<br>AGGGGTCAATTTTGAAGCTCTTG | This paper;<br>Sigma | N/A |
| Zebrafish *h2a.z.2* sgRNA 4<br>target region amplification FP<br>CCCGAGCTGTCTTAATGTGC | This paper;<br>Sigma | N/A |
| Zebrafish *h2a.z.2* sgRNA 4<br>target region amplification RP<br>TGGATTAAAGGATGAACACAAGC | This paper;<br>Sigma | N/A |
| Mitf ChIP FP<br>TTCTGGTCCAAGTCCCAAGC | This paper;<br>Sigma | N/A |
| Mitf ChIP RP<br>ACTTCGAAATCCGCCACGAT | This paper;<br>Sigma | N/A |
| Sox9 ChIP FP<br>CTCGGAACTGCCTGGAAACTT | This paper;<br>Sigma | N/A |
| Sox9 ChIP RP<br>AAAACAGAGAACGAAACCGGG | This paper;<br>Sigma | N/A |
| Sox10 ChIP FP<br>TTCAGGCTCCGTCCAGACAAG | This paper;<br>Sigma | N/A |
| Sox10 ChIP RP<br>CAAGGTGTGCGGTCCAGC | This paper;<br>Sigma | N/A |
| Foxd3 ChIP FP<br>CGTAGAGAAGCGTCGAGGAC | This paper;<br>Sigma | N/A |

| | | |
|---|---|---|
| Foxd3 ChIP RP GTCAGCTCACACGAGGAGG | This paper; Sigma | N/A |
| Pax3 ChIP FP GTCTCCTCCTCGGCCAATCG | This paper; Sigma | N/A |
| Pax3 ChIP RP GGGATCCGGACTAGGGAGC | This paper; Sigma | N/A |
| Sox2 ChIP FP GGCAGAGAAGAGAGTGTTTGC | This paper; Sigma | N/A |
| Sox2 ChIP RP CTTAAGCCTCGGGCTCCAAA | This paper; Sigma | N/A |
| Tfap2a ChIP FP TGTGATTCGCCAGACGCC | This paper; Sigma | N/A |
| Tfap2a ChIP RP GAGACAAAAAGCGAGCGACG | This paper; Sigma | N/A |
| C-kit ChIP FP ATCTGCTCTGCGTCCTGTTG | This paper; Sigma | N/A |
| C-kit ChIP RP GGGTGCAGTCCTCTTGTCTG | This paper; Sigma | N/A |
| Tfap2e ChIP FP CACCCGTTGCCCGACTTTTT | This paper; Sigma | N/A |
| Tfap2e ChIP RP AAGGTACGGGGTACTCAGCG | This paper; Sigma | N/A |
| Dct ChIP FP GGGAGCTTTCGTCTTGCTCT | This paper; Sigma | N/A |
| Dct ChIP RP TCCATTAAGGGCGCATAGCC | This paper; Sigma | N/A |
| Tyr ChIP FP GGGAGGAAAGGGTGCTTGAG | This paper; Sigma | N/A |
| Tyr ChIP RP AGGCTTGGGTTGTAATGCCA | This paper; Sigma | N/A |
| Tyrp1 ChIP FP CCAGTGTGAGGAATCTGGCTTG | This paper; Sigma | N/A |
| Tyrp1 ChIP RP TGCCAGCTGTTAATTGCCCG | This paper; Sigma | N/A |
| mH2a.z.2 A14T oligo GACAGTGGGAAGGCCAAGACTAAGGCG GTGTCTCGTTCC | This paper; Sigma | N/A |
| mH2a.z.2 A14T oligo complement GGAACGAGACACCGCCTTAGTCTTGGCC TTCCCACTGTC | This paper; Sigma | N/A |
| mH2a.z.2 T38S oligo CACAGACACTTGAAGAGTCGCACCACAA GCCATG | This paper; Sigma | N/A |
| mH2a.z.2 T38S complement CATGGCTTGTGGTGCGACTCTTCAAGTG TCTGTG | This paper; Sigma | N/A |
| mH2a.z.2 A127V oligo GGGCAGCAGAAAACTGTTCCCGGGCCC GC | This paper; Sigma | N/A |

| | | |
|---|---|---|
| mH2a.z.2 A127V oligo complement GCGGGCCCGGGAACAGTTTTCTGCTGCCC | This paper; Sigma | N/A |
| | | |
| **Recombinant DNA** | | |
| Mouse H2a.z.2 CDS – Zero TOPO Blunt | This paper | N/A |
| Mouse H2a.z.1 CDS – Zero TOPO Blunt | This paper | N/A |
| Zebrafish mitfa CDS – Zero TOPO Blunt | This paper | N/A |
| pIRES-mouse H2a.z.2 CDS | This paper | N/A |
| Zebrafish *h2a.z.2*-3ÚTR WISH probe construct | This paper | N/A |
| Zebrafish *foxd3* WISH probe construct | Stewart R.A et al; 2006; Dev Biol | N/A |
| Zebrafish *sox10* WISH probe construct | Stewart R.A et al; 2006; Dev Biol | N/A |
| Zebrafish *tfap2a* WISH probe construct | Stewart R.A et al; 2006; Dev Biol | N/A |
| Zebrafish *crestin* WISH probe construct | Stewart R.A et al; 2006; Dev Biol | N/A |
| Zebrafish *sox9a* WISH probe construct | Yan YL et al; 2005; Development | N/A |
| Zebrafish *sox9b* WISH probe construct | Yan YL et al; 2005; Development | N/A |
| Zebrafish *krox20* WISH probe construct | Fiejoo CG et al; 2009; Mol Cell Neuro | N/A |
| Zebrafish *mbp* WISH probe construct | Brosamle C et al; 2002; Glia | N/A |
| Zebrafish *neurod1* WISH probe construct | Rauch G; 2003 | N/A |
| Zebrafish *mitfa* WISH probe construct | Lister JA et al; 1999; Development | N/A |
| Zebrafish *dct* WISH probe construct | Lister JA et al; 1999; Development | N/A |
| Zebrafish *c-kit* WISH probe construct | Parichy DM et al; 1999; Development | N/A |
| Zebrafish *isl2a* WISH probe construct | Asad Z et al; 2016; Hum Mol Genetics | N/A |
| | | |
| **Softwares and Algorithm** | | |

| | | |
|---|---|---|
| R Studio i386 3.5.3 | | N/A |
| Prism 7.0 | Graphpad Software | N/A |
| Reactome PA | Yu G et al; 2016, Mol Biosystem | https://github.com/GuangchuangYu/ReactomePA |
| ImageJ | Schneider et al., 2012 | https://imagej.nih.gov/ij/ |
| | | |